



Composition, frequency, and magnitude of future rain-on-snow floods in Germany

Christian Czakay¹, Larisa Tarasova², and Bodo Ahrens¹

Correspondence: Christian Czakay (czakay@iau.uni-frankfurt.de)

Abstract. In Germany, severe trans-basin winter floods are often generated by rain-on-snow (ROS) phenomena. Under suitable conditions, when rain falls on the snow cover, the snow can melt and produce extreme amounts of runoff. In a warming climate, the frequency of ROS events is expected to change locally depending on elevation and regionally based on the general climate conditions. Consequently, the characteristics of ROS-driven winter floods are also anticipated to change. To investigate these changes, streamflow for multiple gauge stations in Germany was simulated using a deep learning model based on an ensemble of downscaled climate projections. Germany, as a representative mid-latitude country with a considerable portion of historical floods generated by ROS, offers extensive spatial and temporal coverage of hydrological observations spanning long temporal scales, and hence warranting efficient training of the deep learning model. We used explainable artificial intelligence to examine flood-generating processes, focusing primarily on ROS, for every simulated flood peak. Changes in frequency, feature importance, and magnitude of ROS flood events were assessed for individual streamflow gauges and for trans-basin floods across four major river basins in Germany. We found that with regard to the ensemble median, the frequency of ROS floods will decrease at the scale of individual gauges, as well as at the trans-basin scale for the Rhine, Elbe, and Weser River basins but increase in the Danube River basin. For all regions, the snowmelt component during ROS floods becomes less relevant, whereas the contribution of rainfall to these events increases. Interestingly, the severity of both the mean and the most extreme ROS trans-basin floods is projected to increase compared to the historical period in all major river basins in Germany, even though several individual gauges may experience a decrease in magnitude. Despite the overall agreement in the trends of the input features across climate models, the resulting trends in ROS floods are considerably disparate. This discrepancy is primarily attributed to the variations in snow dynamics in different climate models.

1 Introduction

Events in which rain falls on an existing snowpack and generates additional runoff are called rain-on-snow (ROS) events. Such events are very common in mid-latitude regions of the Northern Hemisphere (Cohen et al., 2015) such as the Pacific Northwest USA and Canada (e.g., McCabe et al., 2007; Trubilowicz and Moore, 2017), central and northern Europe, and Eurasia (e.g., Sui and Koehler, 2001; Ye et al., 2008; Pall et al., 2019), and high-mountain regions in Asia (e.g., Ohba and Kawase, 2020; Maina and Kumar, 2023). ROS events can produce large amounts of runoff, making them an important process for flood generation

¹Institute for Atmospheric and Environmental Sciences, Goethe University Frankfurt am Main, Germany,

²Department Catchment Hydrology, Helmholtz Centre for Environmental Research - UFZ, Halle (Saale), Germany

https://doi.org/10.5194/egusphere-2025-3532 Preprint. Discussion started: 10 November 2025

© Author(s) 2025. CC BY 4.0 License.





(Sui and Koehler, 2001; Merz and Blöschl, 2003). Both rainfall and snowmelt can contribute significantly to the generated runoff, with the dominant role varying depending on the location and season (Trubilowicz and Moore, 2017; Li et al., 2019). For the melting process itself, rainfall contributes only a small amount of total energy, while net radiation and turbulent heat fluxes supply most of it (Mazurkiewicz et al., 2008; Li et al., 2019). However, the rainfall plays a critical role by saturating the snow cover and triggering fast runoff (Rössler et al., 2014).

ROS events occur primarily from October to May in low- to mid-elevation regions (McCabe et al., 2007; Cohen et al., 2015), but have also been reported in September and during the summer months, especially in high-elevation regions (McCabe et al., 2007; Morán-Tejeda et al., 2016; Beniston and Stoffel, 2016). With increasing temperatures fueled by global warming, changes in the frequency and magnitude of runoff generated by ROS events, as well as a higher associated flood risk, are expected (Freudiger et al., 2014; Musselman et al., 2018; Chegwidden S et al., 2020). Observations generally indicate an increase in ROS frequency for high-elevation basins, while lower-elevation regions show a decrease, depending on the season (Freudiger et al., 2014; Pall et al., 2019; Ondrej Hotovy and Jenicek, 2023). These studies attribute the change in ROS frequency mainly to an increased frequency of rainfall during the winter half of the year, which is the result of warmer air temperatures, and to the lack of persistence of a pre-existing snowpack.

In recent decades, the frequency and magnitude of floods have changed and are expected to change further in a warming climate (e.g., Petrow et al., 2009; Rojas et al., 2012; Blöschl et al., 2019; Bertola et al., 2020; Huang et al., 2022; Chegwidden S et al., 2020). These changes in the frequency, timing, and magnitude of floods depend on the type of flood and the specific region (Tarasova et al., 2023). Blöschl et al. (2017) demonstrate a spatially heterogeneous trend in flood timings across Europe, finding that floods related to snowmelt tend to occur earlier in the year. Similar to the changes in flood timings, changes in flood magnitude are also spatially heterogeneous across Europe, although clear patterns emerge for regions experiencing an increase or a decrease in flood magnitude (Blöschl et al., 2019).

For the USA, Huang et al. (2022) observe a decrease in the frequency and magnitude of ROS-driven floods during the period from 1960 to 2018. This trend of decreasing ROS-driven floods is projected to continue in an RCP8.5 scenario (Chegwidden S et al., 2020). For an RCP4.5 scenario the decrease in ROS-driven floods is similar in low-elevated basins, but much weaker in mid to high-elevated basins. In contrast, for a future RCP4.5 scenario in Europe, Sezen et al. (2020) find that for two rivers in Slovenia, the frequency of ROS floods will increase, with a peak in the period from 2041 to 2070 along with a generally weaker seasonality. Their results also suggest that the median ROS flood magnitude will decrease, while extremes could become stronger. Also, Beniston and Stoffel (2016) find that for a basin located in Switzerland, a temperature rise of 4-5°C will increase ROS frequency by about 40% at low elevations and 200% at high elevations. However, for temperature increases of more than 5°C, this trend reverses.

Germany, as an example of a mid-latitude country in Central Europe, with rivers of varying elevation that are frequently affected by ROS events (Sui and Koehler, 2001; Freudiger et al., 2014; Tarasova et al., 2020a). The current understanding of changes in ROS events in Germany is fragmented. On one hand, the simulations of ROS events by Dong and Menzel (2020) show a significant reduction of the snow water equivalent (SWE) during winter periods during 1961 to 2016 in Rhineland-Palatinate, a mid-range upland region located within the Rhine basin in Germany. On the other hand, their simulations show that the ROS

https://doi.org/10.5194/egusphere-2025-3532 Preprint. Discussion started: 10 November 2025

© Author(s) 2025. CC BY 4.0 License.





frequency increases in February since the 1990s, while there has been a decrease in January and March. For the major basins in Germany, Freudiger et al. (2014) found an increase in ROS magnitude in upland basins, during the latter half of the period from 1950 to 2011, but at the same time a decrease in ROS frequency in both upland and lowland basins.

Kemter et al. (2020) investigated the relevance of flood-driving mechanisms in Europe and their change for a downscaled reanalysis data set during the time period from 1960 to 2010. They find that soil moisture excess has the largest relevance in northern and middle Germany followed by ROS, snowmelt and stratiform rain. Compared to other regions in Europe, the relevance of flood-generating processes is quite balanced in Germany. Over the Alps, the dominating process is stratiform rain. They find a negative shift in relevance for snowmelt in middle to southern Germany and a positive shift in ROS in these areas. Outside these areas, ROS becomes less relevant. In contrast, the relevance of soil moisture excess increases significantly across Germany. These findings are supported by the findings of Tarasova et al. (2023), who also find a decrease in ROS flood frequency in the time period from 1960 to 2010 and an increase in floods triggered by rainfall on wet soil.

River floods in Germany are often widespread and affect a large part of the river network (Uhlemann et al., 2010) and therefore can have high socio-economic impacts with damages of multiple billion Euros and loss of life (Ulbrich and Fink, 1995; Ulbrich et al., 2003; Petrow et al., 2006; Merz, Bruno et al., 2014, e.g.,). In winter, these floods are often associated with ROS events (Krug et al., 2020). Therefore, the changes projected by previous studies for ROS floods on the catchment scale may also be present on a widespread trans-basin scale. The results of Sezen et al. (2020) show a great variability in terms of projected changes in ROS flood frequency and magnitude between the different climate models. Two different models could project divergent trends in frequency and magnitude of ROS floods for the same emission scenario. This underlines the need of an ensemble-based assessment of trends in flood-generating processes.

The attribution of the generating processes to flood events strongly depends on the method and perspective of the classification (Tarasova et al., 2019). Additionally, Tarasova et al. (2020b) show that a significant part of classification uncertainty originates from the uncertainty of the hydrological model. To overcome the issue of model and classification uncertainty and isolate the variability of climate models, we use a state-of-the-art deep learning approach, Long-Short Term Memory model (LSTM) (Kratzert et al., 2018) to simulate streamflow at multiple gauge stations in Germany. We use these simulations in combination with an explainable artificial intelligence (XAI) technique to interpret the feature importance each simulated flood peak. We then apply a ratio-based classification of the feature importance as suggested by Tarasova et al. (2020b) to identify ROS-generated floods in a large ensemble of climate simulations under the high-emission RCP8.5 scenario.

2 Data and Methods

2.1 Study area and training data

We consider 97 streamflow gauges (Fig. 1) located in the German parts of the Rhine, Danube, Elbe, and Weser River basins.

The gauges were selected based on the availability of daily river discharge and corresponding watershed boundaries from the Global Runoff Data Centre (GRDC) data set (https://grdc.bafg.de/), as well as based on the availability of classification of flood peaks based on their generation processes from the previous study of Tarasova et al. (2020b). Only gauges with a daily





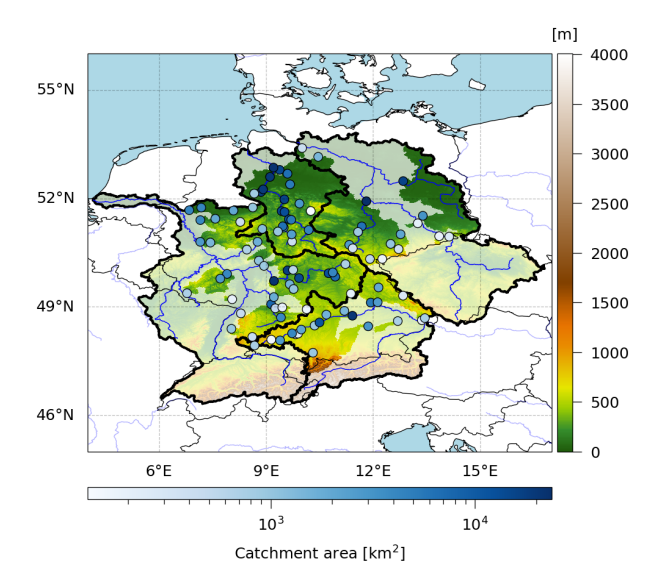


Figure 1. Study area and gauge stations. The thick black outlines show the Germany affecting parts of the 4 major river basins of the Rhine, Danube, Elbe and Weser rivers. The gauge stations are represented by the circles, with the blue color scale representing their basin area. The non-transparent parts of the major river basins are covered by the gauge stations. The elevation data is taken from the ETOPO Global Relief Model (NOAA National Centers for Environmental Information, 2022).

river discharge observation time series and available watershed boundaries from the Global Runoff Data Centre (GRDC) data set (https://grdc.bafg.de/) were included. The time series of 72 gauge stations begin in 1950, 13 in the 1950s, 9 the 1960s, and 3 in the 1970s. The sizes of the study catchment areas range from 127 and 23,719km².

The deep learning model was trained using the ERA5 reanalysis data set (Hersbach et al., 2020) to simulate observed streamflow. The input features included catchment-averaged near surface temperature, liquid precipitation, snowfall, snowmelt, snow amount, surface runoff, subsurface runoff and day length. Liquid precipitation was calculated by subtracting snowfall from total precipitation, while subsurface runoff was determined by subtracting surface runoff from total runoff.

2.2 Deep learning model

100

105

Streamflow was simulated using a Long-Short-Term Memory (LSTM) model (Hochreiter and Schmidhuber (1997)) with the base setup as described in Jiang et al. (2022a) and Jiang et al. (2022b). The model consists of a single LSTM layer with 32 neurons and a dense layer with 1 neuron. An adaptive learning rate, the adaptive moment estimation (Adam) optimizer (Kingma and Ba, 2017), and a batch size of 1024 were selected for model training. The past 150 time steps (in this case, 150 days) were used to simulate river discharge for each day in the time series.

For each individual gauge, 10 independent LSTM models were trained using different segments of the time series by applying





10-fold cross-validation. The performance of the LSTM on the test segments was measured using the Nash-Sutcliffe Efficiency (NSE) (Nash and Sutcliffe, 1970).

As Kratzert et al. (2018) demonstrate, a regionally-trained LSTM outperforms an LSTM trained for individual catchments. However, Jiang et al. (2022a) point out that a regionally trained LSTM can complicate the interpretability of flood-generating processes. For this reason, we opt for individually trained LSTMs in this study.

2.3 Identification of flood-generating processes

events mainly driven by rainfall or snowmelt:

For the identification of flood peaks, a simple peak over threshold (POT) method was applied to all discharge time series. The threshold was set to detect an average of 5 peaks per year. Peaks detected using the POT method are referred to as POT5 peaks. Every peak exceeding the discharge of the flood with a return period of 2 years (Q2) is considered a flood event. Similarly to Jiang et al. (2022a), the flood-generating processes of the discharge peaks were analyzed using the XAI method integrated gradients (IG) (Sundararajan et al., 2017). This method interprets the model gradients used for predictions, providing the importance of each feature for each time step in predicting a single time step of the target variable. In this case, at a given time step (e.g., the date corresponding to a flood peak), the IG method computes 150 values (corresponding to the number of time steps used for prediction) for each input feature (i.e., 7 atmospheric variables and day length). Since our focus is particularly on ROS floods, we only utilized liquid precipitation, snow amount, and snowmelt (i.e., input features that directly relate to the generation of ROS events) for the XAI analysis. However, it is important to note that all other input variables are crucial for the reliable performance of LSTM (i.e., removing any of them results in inferior model performance). All IG values were normalized to account for the different scales of the input features and to enhance comparability between the different peak magnitudes and gauges. Finally, a discharge peak was defined as ROS-driven if the proportion between the sum of absolute IG values of snowmelt (IG_{sm}) and snow amount (IG_{snw}) , and liquid precipitation (IG_{prl}) was between 0.1 (very low importance of snowmelt and very high importance of liquid precipitation for flood generation) and 10 (very high importance of snowmelt and very low importance of liquid precipitation for flood generation) to exclude flood

$$IG_{ROS} = \frac{\sum_{n=0}^{4} |IG_{sm}| + |IG_{snw}|}{\sum_{n=0}^{4} |IG_{prl}|}$$
(1)

$$0.1 < IG_{ROS} < 10$$
 (2)

An IG_{ROS} value of 1 indicates equal importance for both features to the LSTM. We further investigate the suitability of the selected thresholds (see Result Section).

Generally, the values of IG_{prl} and IG_{snm} were positive (indicating that high liquid precipitation and snowmelt were important), while the values of IG_{sm} were negative (indicating that a reduction in snow amount was important). Consequently, the absolutes of the IG values were used for further calculations. To calculate IG_{ROS} for a given time step, the IG values were



140

160



selected from a window of 5 time steps (the current and the past four time steps). This window was selected based on the linear correlation between the resulting IG_{ROS} values for the ERA5-driven simulated discharge peaks and the actual ratio of the snowmelt and liquid precipitation variables from ERA5 (see Fig. A1) and its suitability was further tested (see Results Section).

The XAI-based classification of flood events is evaluated using classified events from Tarasova et al. (2020b) as a benchmark. They used high-resolution (1km) observational precipitation and snowmelt simulated by a regionally calibrated hydrological model (4km). According to their definition, for a ROS event, both the ratio between total event snowmelt and the sum of total event snowmelt and rainfall (to exclude snowmelt floods) and the ratio between total event rainfall and the sum of total event snowmelt and rainfall (to exclude rainfall events) must be lower than 0.95. Additionally, they distinguished between ROS and spatially unrelated rainfall and snowmelt. As we do not have information on the spatial distribution of rainfall and snowmelt due to the catchment-averaging, both cases will be treated as ROS. As a measure of classification quality, multiple skill scores will be considered.

150 Accuracy is defined as the ratio of correct classifications to total classifications:

$$ACC = \frac{TP + TN}{TP + TN + FP + FN} \tag{3}$$

Correct classifications are called true positives (TP) and true negatives (TN). False classifications are named false positives (FP) and false negatives (FN).

Precision is defined as the ratio of true positives and all detected positives (the sum of true positives and false positives):

$$155 \quad PRE = \frac{TP}{TP + FP} \tag{4}$$

Recall is defined as the ratio of true positives and all actual positives (the sum of true positives and false negatives):

$$REC = \frac{TP}{TP + FN} \tag{5}$$

As we aim for the best possible match under consideration, that the frequency of ROS and non-ROS is not equal, the F1 score is used to balance false positives and false negatives. The F1 score is the harmonic mean of precision and recall and defined as:

$$F1 = \frac{2TP}{2TP + FP + FN} \tag{6}$$

For all scores, a value of 1 indicates a perfect classification.

2.4 Trans-basin floods

As trans-basin winter floods in Germany are often driven by ROS events (Krug et al., 2020), the changes in flood-generating processes for trans-basin floods are investigated in addition to those for individual gauges. To identify trans-basin floods, the severity of flood events from all gauges within an 11-day window throughout the entire time series was calculated similarly to the method described by Uhlemann et al. (2010):





$$S = \sum_{i \in \Omega} \left\{ \lambda_i \times \frac{Q_i^P}{\kappa} \right\} \quad ; \ Q_i^P \ge \kappa \tag{7}$$

The severity S is defined as the sum over all gauges affected by a discharge peak (with discharge Q_i^P) that exceeds the flood with a return period of 2 years ($\kappa = Q_2$). Unlike in Uhlemann et al. (2010), the weight factors λ_i represent the catchment area rather than the length of the river network within a catchment. In the case of nested catchments, the weights of the catchments were adjusted according to their areas. The severity peaks were then identified in the resulting severity time series and defined as the trans-basin flood events. A 10% threshold of affected basin area was applied as the minimum required area to identify a trans-basin flood. Furthermore, for a trans-basin flood to be considered a ROS trans-basin event, a minimum of 30% of the affected basin area (i.e., the total area of all catchments with a flood event within a major river basin during a trans-basin flood) must be affected by ROS floods. We examined the effect of this threshold by varying it from a very low ROS contribution (i.e., at least one gauge has to be affected by ROS) to more substantial ones (i.e., 50% of the area must be affected by ROS). Our preliminary tests showed that while some of the absolute values of trans-basin ROS flood properties (e.g., the number of trans-basin ROS floods) vary depending on the selected threshold, the projected changes for future climate scenarios remain.

180 2.5 Climate simulations

To analyze changes in the flood-generating processes of ROS floods, the ERA5-trained LSTM was used to simulate stream-flow for 31 downscaled CORDEX CMIP5 historical and high-emission RCP8.5 climate simulations (available at https://esgf-metagrid.cloud.dkrz.de/). An overview of all selected combinations of global and regional climate models (GCM and RCM) is provided in Table A1. For climate simulations downscaled with the ALADIN63, HIRHAM5 and RACMO22E models, glacial areas were masked to avoid erroneous interpretations of snowmelt dynamics in these regions. The GCM-RCM simulations were bias-corrected using quantile delta mapping (Cannon et al., 2015).

In addition to the climate scenarios, streamflow was also simulated using the LSTM for the ERA-Interim-driven (Dee et al., 2011) evaluation runs for each RCM. This provides information on the ability of downscaled reanalysis (i.e. ERA-Interim-RCM) to reproduce the results produced by raw reanalysis (i.e., ERA5) when training the LSTM and driving the ERA5-trained LSTM and can reveal the impact of the RCM induced biases in climate simulations on streamflow modeling when driving or training the LSTM. For the evaluation runs, the streamflow was simulated in three different ways:

- 1. Using the raw ERA-Interim evaluation run to drive the ERA5-trained LSTM to show the full impact of RCM induced biases for downscaled reanalysis on streamflow simulation.
- 2. Training the LSTM with the raw ERA-Interim driven evaluation run (instead of ERA5) and simulate the streamflow for the raw ERA-Interim evaluation run. In this way, the LSTM learns the characteristics and thus the biases of the ERA-Interim-RCM system. Assuming an accurate spatial and temporal representation of, e.g., precipitation events in the

https://doi.org/10.5194/egusphere-2025-3532 Preprint. Discussion started: 10 November 2025

© Author(s) 2025. CC BY 4.0 License.



200

205

210

215



downscaled reanalysis, the ERA-Interim-RCM-trained LSTM has the potential to outperform the ERA5-trained LSTM while internalizing the RCM biases and enhancing the quality of the GCM-RCM-driven streamflow simulations.

3. Using the bias-corrected ERA-Interim evaluation runs to drive the ERA5-trained LSTM to reduce the impact of RCM induced biases on streamflow simulation from the first case.

For the climate scenarios, the changes in ROS flood frequency, the importance of snowmelt, mean and maximum flood magnitudes, mean flood timing, and, specifically for trans-basin floods, the total ROS-affected basin area were calculated. Changes in flood magnitudes were assessed by ranking all flood events for each gauge and each simulation over the entire period of 1950 to 2100. These ranks were then normalized to a value between 0 and 1 to account for the varying numbers of ROS floods produced by the LSTM driven with different climate models. As LSTMs are known to perform poorly when extrapolating events which they have not seen during training, magnitudes of future extreme floods and the resulting changes in magnitude can potentially be heavily underestimated (e.g., Song et al., 2025). We try to overcome this issue by applying the ranking and stating if flood magnitude increases rather than by how much (e.g., the magnitude of a future flood may be heavily underestimated, but it still ranks highest). Consequently, instead of the usual 30-year period used for climate, the time series were divided into four overlapping 60-year periods to mitigate the influence of rare and extreme floods on the assessment of flood magnitude changes. The period from 1951 to 2010 is defined as the reference period (REF), while the periods from 1981 to 2040, from 2011 to 2070 and from 2040 to 2100 are referenced as 1981-2040, 2011-2070 and 2040-2100, respectively. All properties and trends were calculated individually for each GCM-RCM-driven simulation. For each gauge, the ensemble median was calculated as the median of trends. The significance of the trends (P < 0.05) was determined by applying the Mann-Whitney U test (Mann and Whitney, 1947) to the ensemble.

To gain further insight into potential changes in ROS floods, changes in various aggregations of the variables used for ROS classification (and related variables) (i.e. snow amount, snowmelt, snowfall and liquid precipitation) were evaluated as well (see Table 1). The 5-day sums for calculating extremes were chosen based on the 5-day window for the XAI.

220 3 Results and Discussion

In the first part, the simulation quality of the LSTM models is evaluated, and the identified flood events and flood-generating processes are compared with the results of previous studies. In the second part, the properties of ROS floods and their changes are analyzed and discussed for climate projections.

3.1 Evaluation of the LSTM simulations

225 3.1.1 ERA5-based training

Figure 2 shows the performance of the LSTM in relation to the size of the gauge station catchments. The simulation accuracy is relatively high for the vast majority of gauges (i.e., 94 out of the 97 gauges have a NSE of at least 0.5), with particularly strong performance for larger catchments. The lower performance for catchments with an area smaller than 600 km^2 is likely





Table 1. Calculated quantities

| value | period | |
|--|----------------|--|
| mean annual maximum snow amount | whole year | |
| maximum snow amount | whole year | |
| mean annual snow days $(SWE > 15 mm)^1$ | whole year | |
| mean annual maximum 5-day snowmelt | October to May | |
| maximum 5-day snowmelt | October to May | |
| mean annual snowfall amount | October to May | |
| mean annual maximum 5-day snowfall | October to May | |
| maximum 5-day snowfall | October to May | |
| mean annual liquid precipitation amount | October to May | |
| mean annual maximum 5-day liquid precipitation | October to May | |
| maximum 5-day liquid precipitation | October to May | |
| mean ROS water ² | whole year | |
| maximum ROS water ² | whole year | |
| number of ROS events ³ | whole year | |
| | | |

¹A gid cell is considered as fully covered by snow if the snow amount exceeds 15mm SWE. ²ROS water is here defined as the sum of 5-day liquid precipitation and snowmelt if both ratios of both quantities are larger than 0.1. The ratio of 0.1 was chosen based on the ratios of the XAI-based classification. Note, that the values cannot be translated 1:1 and the LSTM values snowmelt more than liquid precipitation (see Fig. A1 (b)). However, the results do not change, if a less strict ratio (i.e., 0.01) is applied.

³If conditions of ² are met.

attributed to the coarse spatial resolution of ERA5.

240

Additionally, the variable performance of the LSTMs can be linked to anthropogenic activities, such as dams and reservoirs. For example, the Müglitz River at Dohna presents an extreme case with an average NSE of only 0.09. In recent decades, two flood control reservoirs have been constructed in the Müglitz River, potentially disturbing the relationship between the atmospheric variables, which are considered as input variables in our model setup, and the observed discharge. Since a low performance of the deep learning model inevitably affects the interpretability of explainable machine learning approaches (Stein et al., 2021), we exclude this gauge from further analysis.

The ERA5-driven LSTM generally also shows good agreement in terms of observed flood peak simulations. Figure 3 illustrates the accuracy of detecting POT5 peaks and floods ($Q > Q_2$) for all individual gauges in the ERA5-driven streamflow simulations of the LSTM model compared to the observations. A POT5 peak or flood is counted as true positive if the dates of the observed and simulated peaks are not more than 3 days apart. The dates of POT5 peaks did matched or were shifted by only 1 day on average for about 80% to 95% for 85 out of 96 gauges. For the remaining 11 gauges, up to 60% of POT5 peaks





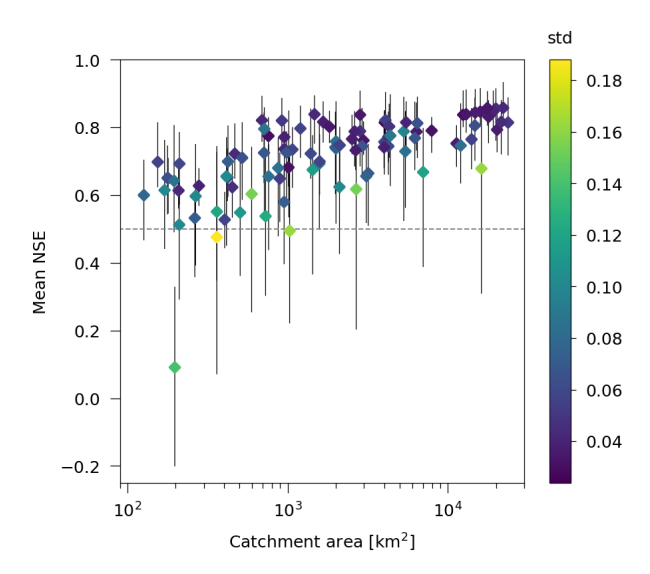


Figure 2. The NSE performance of the 10 individually trained LSTMs for the test segments of the time series for streamflow simulation for each river gauge depending on the catchment area. The black lines represent the best and worst of the LSTM ensemble. The color shows the standard deviation (std) of the 10 individual LSTMs.

exhibited a time shift of 2 or 3 days. The accuracy of POT5 peak identification generally lies between 60% and 85% for 91 gauges. For flood detection, the accuracy is slightly lower with values ranging from 35% to 80%.

The observational POT5 peaks are both underestimated and overestimated in the ERA5-driven simulation, with the majority being underestimated (Fig. 4). The ability of the ERA5-driven LSTM model to simulate floods, particularly their timing, warrants further investigation into changes in flood-generating processes using XAI, even if the magnitudes of the corresponding events are underestimated or overestimated (Tarasova et al., 2023).

The adapted definition of trans-basin floods successfully reproduces most of the detected trans-basin floods from Uhlemann et al. (2010). During the period from 1952 to 2002, 104 trans-basin floods were identified in the observations. Out of the 80 trans-basin floods documented by Uhlemann et al. (2010), only 15 were not identified in our simulations, with most of the missing widespread floods occurring in summer (80%). Nevertheless, the higher-ranked trans-basin floods are well represented (Table S1). Moreover, certain events might not be captured due to the differences in the considered gauges and in the definition of trans-basin floods used in this study and in the study of Uhlemann et al. (2010) (i.e., weighting of gauges by catchment area rather than the length of the river network, as well as different flood thresholds).

The ERA5-driven LSTM simulation appears to represent trans-basin floods effectively (Fig. 5(a)). From 1951 to 2015, 127 trans-basin floods were detected in the observations and 119 in the ERA5-driven simulation. Of the 127 detected floods in the observations, 98 were identified in the ERA5-driven simulation.

Most trans-basin floods occurred between December and March for both the observations and the ERA5-driven LSTM simu-





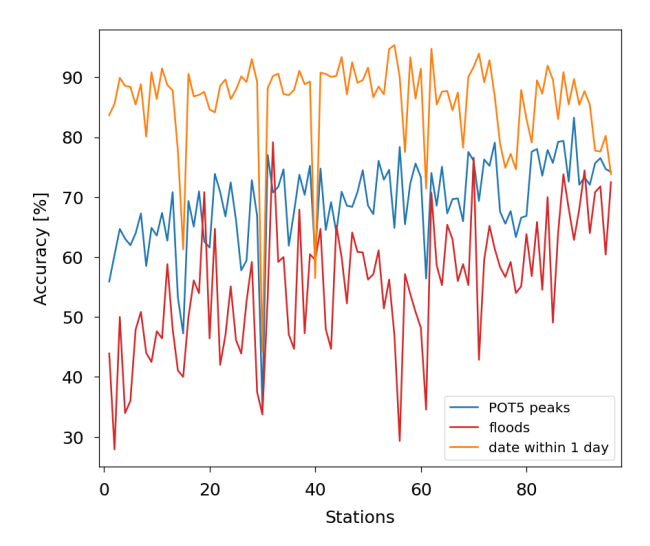


Figure 3. Percentage of detected POT5 peaks and floods $(Q > Q_2)$ of the observations that were detected in the test segments of the ERA5-driven simulations of the LSTM model and the percentage of POT5 peaks which had the same peak date or a date shifted by only 1 day. The gauges are sorted by their average NSE-based performance of the LSTM model for simulating observed streamflow time series.

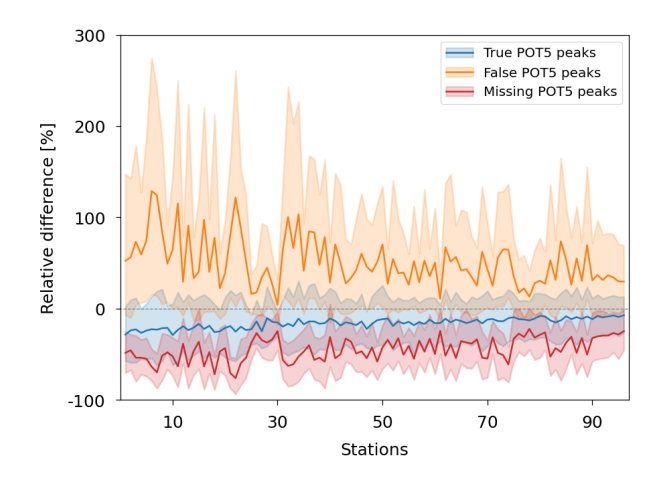


Figure 4. Relative differences in magnitudes between observational POT5 peaks and the simulated POT5 peaks from the ERA5-driven simulation. Differences are shown for POT5 peaks, that are present in both time series (true POT5), POT5 peaks which are detected in the ERA5-driven simulation but not in the observations (false POT5), and POT5 peaks which were detected in the observations but not in the ERA5-driven simulation (missing POT5).

lation (Fig. 5 (b)). The number of trans-basin floods between June and October is lower in the ERA5-driven simulation than in the observations. Additionally, the number of trans-basin floods in summer and autumn is considerably lower than for winter



265



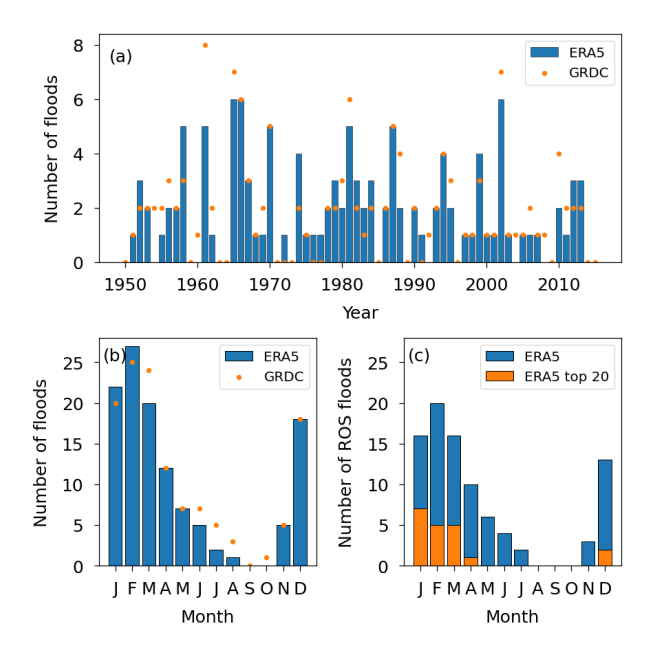


Figure 5. Time series of trans-basin flood frequency for the ERA5-driven LSTM simulation and the GRDC observations (a), temporal distribution of trans-basin floods for the ERA5-driven simulation and the GRDC observations (b) and seasonal distribution of trans-basin ROS floods including the 20 highest ranked ROS floods for the ERA5-driven simulation (c).

and spring for both time series. The distribution of trans-basin ROS floods for the ERA5-driven LSTM simulation (Fig. 5 (c)) shows that most trans-basin floods in Germany are (at least partly) ROS-driven. Furthermore, no trans-basin ROS floods were detected between August and October for the ERA5-driven simulation. The top 20 highest-ranked ROS floods in the ERA5-driven simulation mainly occurred from January to March with only three of these floods happening in December (2) and April (1).

A comparison of flood-generating processes for individual gauges between the XAI-based interpretation of the ERA5-driven simulation and the attribution by Tarasova et al. (2020b) shows that a time window of 5 days for feature attribution in the XAI-based classification and a minimum IG_{ROS} of 0.1 as a lower limit for ROS floods yield the best results (Fig. 6). While accuracy and precision achieve optimal results for longer time windows and higher minimum ROS thresholds, recall exhibits the opposite trend. This discrepancy is attributed to the higher proportion of rainfall-driven floods in Tarasova et al. (2020b) compared to the results from the ERA5-driven simulation of this study. Increasing the minimum thresholds for ROS floods increases the number of non-ROS floods, thereby enhancing accuracy and precision. The resulting F1 score, which balances precision and recall, is highest for windows larger than 4 days (as suggested by the correlation in Fig. A1) and lower minimum IG_{ROS} thresholds. The primary difference from the results from Tarasova et al. (2020b) can be linked to the different data sets used for flood process attribution. They used high-resolution (1km) precipitation and snowmelt simulated by a regionally calibrated



280

290

295



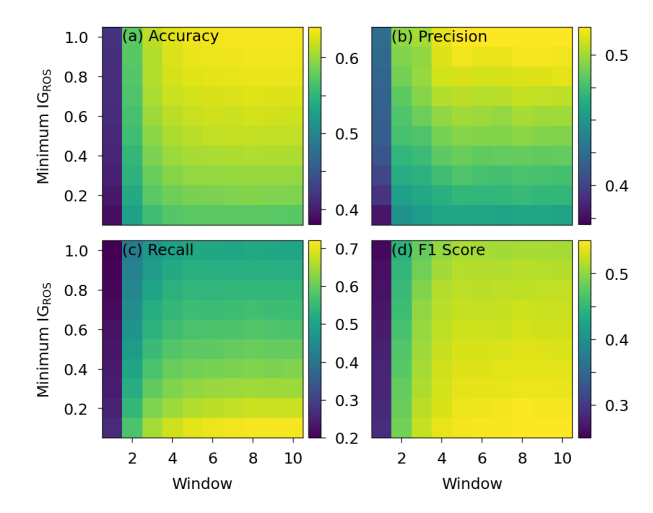


Figure 6. Comparison of ROS and non-ROS floods according to the classification of Tarasova et al. (2020b) using interpolated observed precipitation and snowmelt simulated by a regionally calibrated hydrological model and the XAI-based classification of floods using ERA5-driven simulations of the LSTM model from this study. Accuracy (a), precision (b), recall (d), and F1-score (d).

hydrological model (4km). For a minimum IG_{ROS} of 0.1 and across all gauges, a snowmelt peak was present in ERA5 for 98% of all POT5 peaks classified as rainfall-driven according to Tarasova et al. (2020b). This discrepancy likely arises from the coarse resolution of ERA5, which could lead to an inaccurate representation of snowmelt processes, particularly for smaller basins. However, no relationship was found between the F1 score and the basin area.

The results indicate that the ERA5-driven LSTM simulation and the XAI-based classification of ROS floods can effectively reproduce the findings of previous observation-based studies.

3.1.2 ERA-Interim-driven simulations

The ERA5-trained LSTMs driven by the raw output from the CORDEX evaluation runs (RCM-ERA-Interim) fail to accurately reproduce streamflow dynamics in the study area (Fig. 7 (a)), with almost all models performing rather poorly (i.e., negative NSE for nearly all gauges). In particular, the LSTM runs driven by the outputs from HIRHAM5 and ALADIN63 perform very poorly.

In contrast, the LSTMs trained on the raw CORDEX evaluation runs show considerably better performance (Fig. 7 (b)). Although this performance improves considerably, it remains inferior to that of simulations trained and driven by ERA5. While peak flows are underestimated, the overall representation of the streamflow dynamics is greatly improved (Fig. 7 (e)).

Using the bias-corrected output from the CORDEX simulation runs to drive the ERA5-trained LSTM massively improves the performance of the streamflow simulation compared to the raw evaluation runs. This improvement in performance is comparable to the improvement achieved by training the LSTM directly with the evaluation runs instead of ERA5 (Fig.7 (c)). Because training of an LSTM for each individual RCM has a much higher computational cost compared to bias-correction of the data



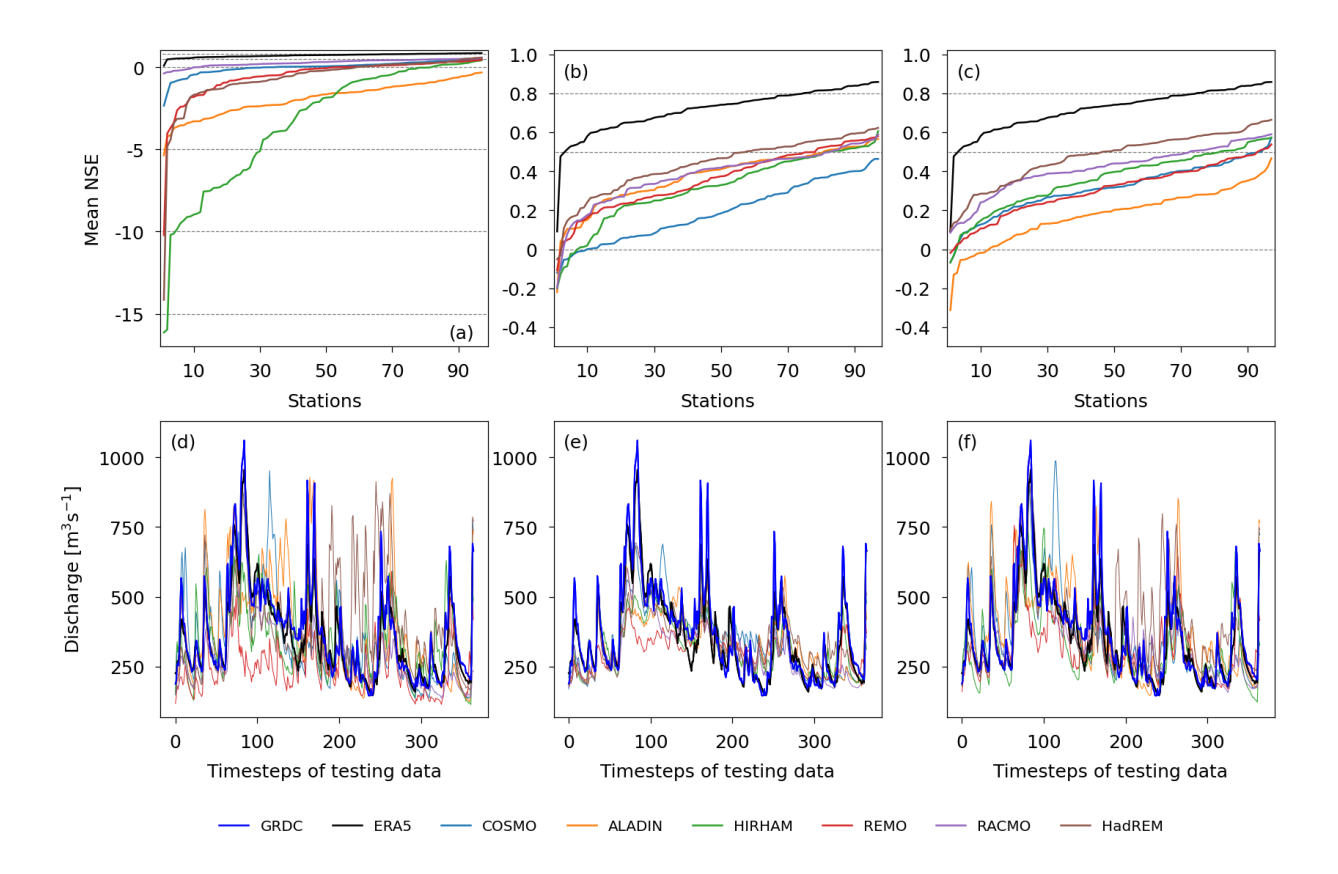


Figure 7. Streamflow simulation accuracy of the ERA5-trained LSTM driven by the raw RCM-ERA-Interim (a and d), the RCM-ERA-Interim (a and d), the RCM-ERA-Interim (b and d) and the ERA5-trained LSTM driven by the bias-corrected RCM-ERA-Interim (c and f). The top panel shows the mean NSE of the streamflow simulations for each basin. The lines are sorted from worst to best performing model. The bottom panel shows an example of the resulting predicted discharge for 365 time steps of the testing data for the Ingolstadt station. The GRDC observations and the simulated ERA5-driven discharge are added as reference.

and does not greatly improve the performance of the simulation, we prefer the latter method in this study.

3.1.3 Historical period of RCM-GCM-driven simulations

300

To evaluate the simulation quality of the climate projections, the climatology for the REF period is compared with GRDC observations for the 31 GCM-RCM-driven and ERA5-driven simulations. The ensemble median annual streamflow closely aligns with the GRDC observations (Fig. 8). For most gauges, it is overestimated by up to 15% for the ensemble median and 25% for the 90th percentile. Only at eight gauges is the mean streamflow underestimated in the median, and to a lesser extent. In contrast, for the ERA5-driven simulation, the mean streamflow is underestimated in more cases than it is overestimated.



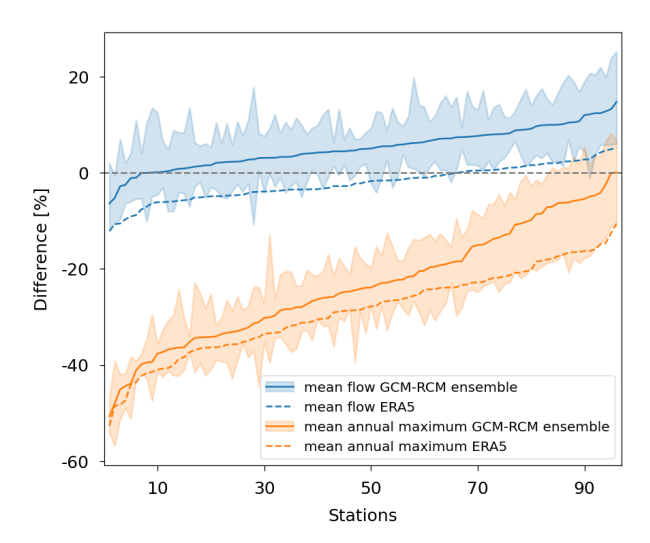


Figure 8. The climatological difference for mean streamflow and mean annual maxima between the ensemble of the RCM-GCM-driven simulations and the GRDC observations, and between the ERA5-driven simulation and the GRDC observations. The stations are sorted by the amount of difference separately for each line.

The mean annual maxima are consistently lower by up to 50% for the ensemble median and are only overestimated for a few gauges within the 10th to 90th percentiles. The mean annual maxima for the ERA5-driven simulation show even higher underestimation than those for the ensemble median. Overall, the ERA5-trained LSTMs can produce realistic streamflow when driven by climate projections.

3.2 Projected changes for rain-on-snow floods

In the following section, we present the changes in ROS floods for the four examined time periods. These changes are analyzed first separately for the individual gauges and then at a trans-basin scale for the four major river basins of the Rhine, Danube, Elbe, and Weser rivers. The figures shown in this section focus mainly on the changes in the GCM-RCM ensemble median. Figures illustrating the changes for the individual models can be found in the supplementary materials.

3.2.1 Individual gauges

The results and trends of ROS floods for the individual gauges are shown in Fig. 9. Figure 10 (Figs. S1 and S2) adds spatial context for the changes projected for the ensemble median for the periods 2041-2100 (1981-2040 and 2011-2070). For the 1981-2040 period, there is an overall slight increase in ROS flood frequency for the ensemble median (Fig. 9(a), Fig. S1(a)). Starting in the 2011-2070 period, the ROS flood frequency decreases for most gauges (Fig. S2(a)), while 13 gauges experience an increase. In particular, for the 2041-2100 period, some gauges exhibit an extreme increase in numbers, whereas for most gauges, a moderate to high decrease is projected (Fig. 9(a)). The gauges with an increasing number of ROS floods are located





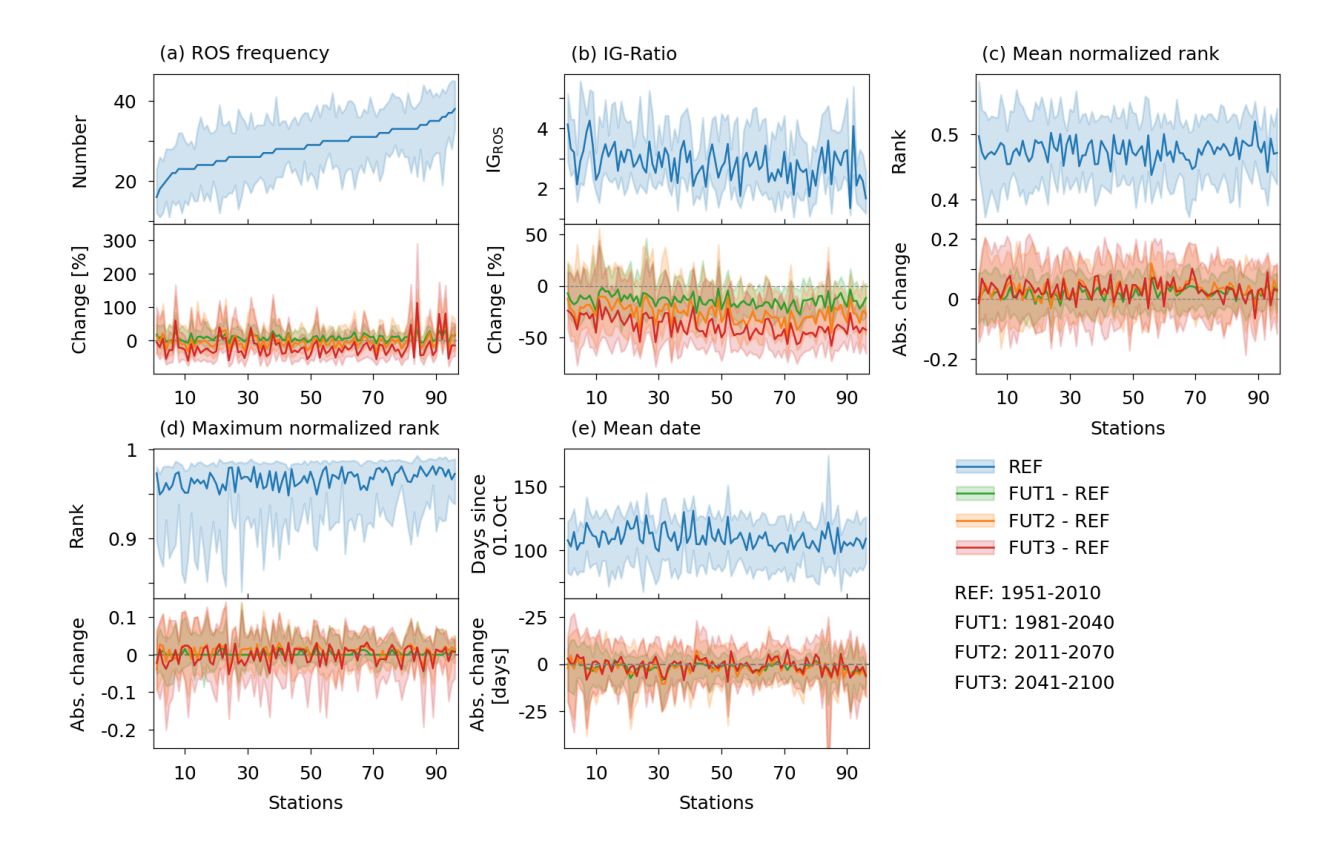


Figure 9. Number of ROS floods and their properties for 4 time periods. The top panel shows the number of ROS floods (a), the XAI-based snowmelt importance IG_{ROS} (b), the mean normalized rank (c), the maximum normalized rank (d) and the mean ROS flood date (e) for the GCM-RCM ensemble median for the reference period REF. The shaded areas represent the 10th to 90th percentile of the RCM ensemble. The lower panels show the relative changes for 3 future time periods with regard to the reference period. The gauges in all panels are sorted by the median number of ROS floods.

in the northwestern part of the Danube River Basin, as well as the midwestern part of the Elbe River Basin (Fig. 10(a)). In these basins, some catchments are associated with higher elevations compared to the Rhine and Weser River basins. Apart from one gauge in the Danube River basin that shows an increase of up to 113% for the ensemble median, the increase for all other gauges falls within the range of -60% and +80%. For the 10th to 90th percentiles these values range from -78% to +175% (Fig. 9(a)).

For the REF period, snowmelt is 2-4 times more important for the LSTM predictions than liquid precipitation during ROS floods in the ensemble median (Fig. 9(b)). The IG_{ROS} values are generally lower for gauges with a higher ROS flood frequency. The importance of snowmelt decreases for all gauges throughout all periods, by up to 57% for the ensemble median and 78% for the 10th to 90th percentiles for the 2041-2100 period.

Figure 9(c) shows ensemble median of the mean normalized rank of ROS floods. For all future periods, the mean normalized



335

340

345

350

355



rank increases for most gauges, with a generally higher increase for distant futures for the ensemble median. However, the spread of the models increases considerably after the 1981-2040 period. There are only a few individual gauges that experience a decrease in mean rank (Fig. 10(c)).

The maximum rank (Fig. 9(d)) does not reach the value of 1 for the 10th to 90th percentiles in the REF period for any of the gauges. This means that the largest flood is always found within one of the future periods. While for the 1981-2040 period the maximum rank appears to be higher for most of the gauges, more gauges also see a decrease in the maximum rank for the 2011-2070 period, and especially for the 2041-2100 period. The eastern part of the Rhine, western part of the Danube, middle to northern parts of the Weser, and western part of the Elbe River basins contain most of the gauges with a projected increase in maximum flood rank for the 2041-2100 period (Fig. 10(d)). Gauges with a projected decrease in maximum flood rank are mainly located in the middle and western parts of the Rhine, the southern part of the Weser, and the northeastern part of the Danube River basins. For the 1981-2040 period, the maximum rank is always at least as high as for the REF period (Fig. S1(d)). The pattern of the projected changes for the 2010-2070 period (Fig. S2(d)) appears similar to the changes for the 2041-2100 period. However, more of the gauges still show an increase in maximum flood rank, and the projected decreases in maximum flood rank are less pronounced.

There is a clear pattern for the change in average ROS flood timing, with earlier occurrences in the south and east of Germany and later occurrences in the northwest for the ensemble median for the 2041-2100 period (Fig. 9(e)). In central Germany, there is a transition zone with only minor shifts in mean ROS flood date. The average time changes for the ensemble median are generally very small, within ± 10 days for the 2041-2100 period, but can be as large as ± 25 days for models within the 10th and 90th percentiles. The same pattern is already visible for the 1981-2040 and 2011-2070 periods.

Generally, the patterns of projected changes from most of the climate models align with the ensemble median (Figs. S3-S7). In terms of ROS frequency, most models agree on an increase in the Danube River basin and in the western parts of the Elbe River basin, although to varying extents. Some models also project an increase in the Weser River basin, which is not reflected in the ensemble median. In some cases, an extreme increase in ROS flood frequency across large parts of Germany is projected. This behavior is particularly evident in the CNRM-CERFACS-CNRM-CM5-driven RCMs and the GCMs downscaled by the KNMI-RACMO22E model. With regard to changes in the importance of snowmelt, all models agree on a decreasing trend. For most models, some individual gauges, which are spatially heterogeneously distributed within all major river basins, show an increasing trend. The patterns of changes in mean and maximum rank also differ from model to model, but the magnitude of changes is similar across simulations. For flood timing changes, the patterns for many models again appear very similar to the ensemble median. However, there are also models which project a shift to later timings for all of Germany or the opposite. Possible reasons for the differences in trends are discussed at the end of this section.

17





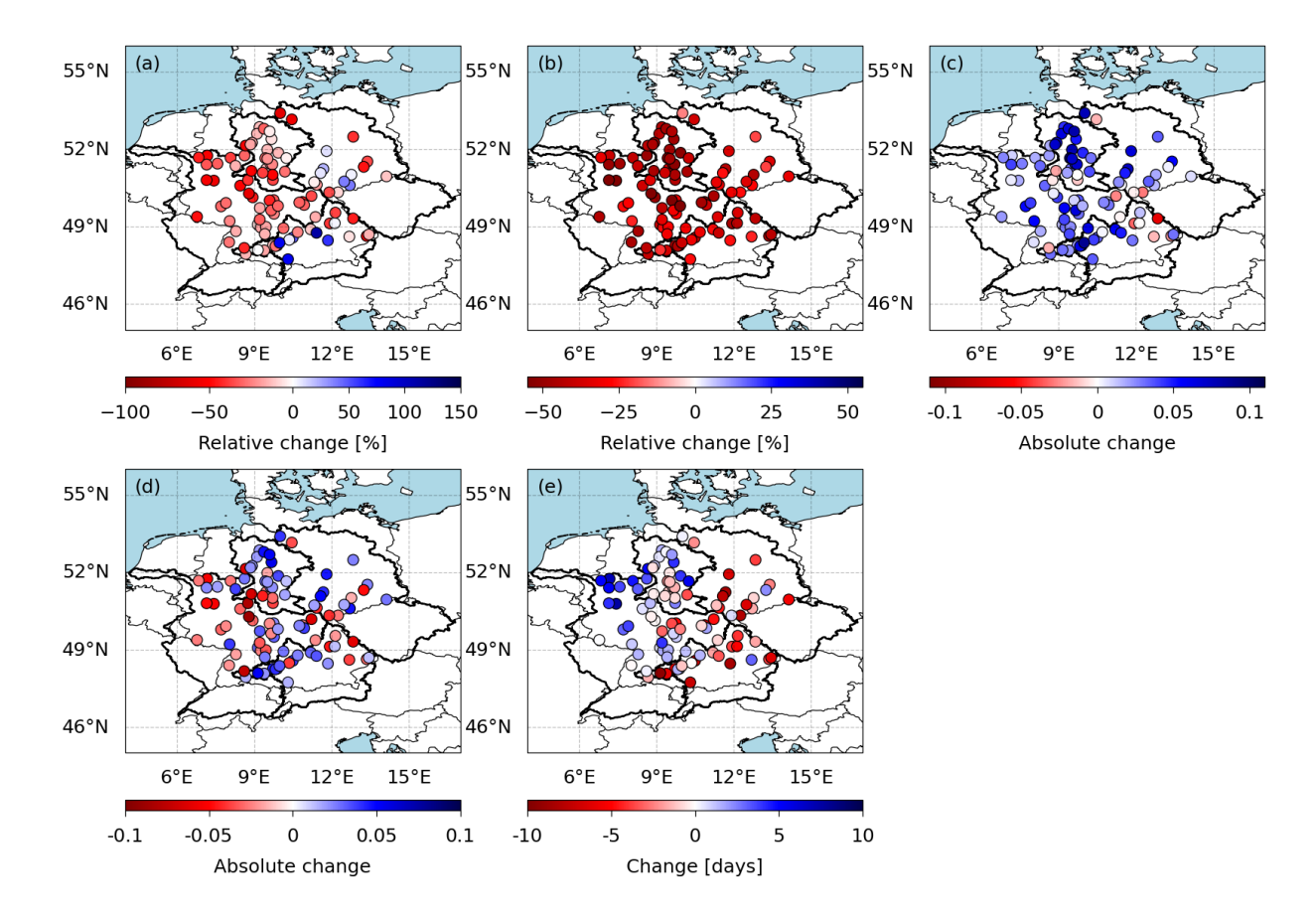


Figure 10. Changes in the number of ROS floods (a), the IG_{ROS} (b), the mean normalized rank (c), the maximum normalized rank (d) and the mean date (e) at all gauges for the GCM-RCM ensemble for the future period 2041-2100 with regard to the reference period.

3.2.2 Trans-basin floods

365

370

A similar picture to that projected for the individual gauges emerges for the trans-basin floods. The trans-basin floods were identified separately for the Rhine, Danube, Elbe, and Weser River basins, as well as for all basins combined. For the Rhine River basin, the number of ROS floods is decreasing throughout all periods (Fig. 11 (a)). The Elbe River basin experiences an increase until the 2011-2070 period, before facing a decrease in ROS flood numbers in the 2041-2100 period. For the Weser River basin, this decline begins already after the 1981-2040 period. Only the Danube River basin shows an increasing trend in ROS flood frequency throughout all periods. When all regions are combined, the numbers increase until the 1981-2040 period and then decline. For the Danube River basin and the combined basins, the model spread increases significantly towards the distant future periods. The projected changes for the 2041-2100 period are significant (P < 0.05), except for the Elbe River basin, due to the decline in ROS numbers after the 2011-2070 period. However, for the Elbe River basin, the change for the 2011-2070 period is significant.



380



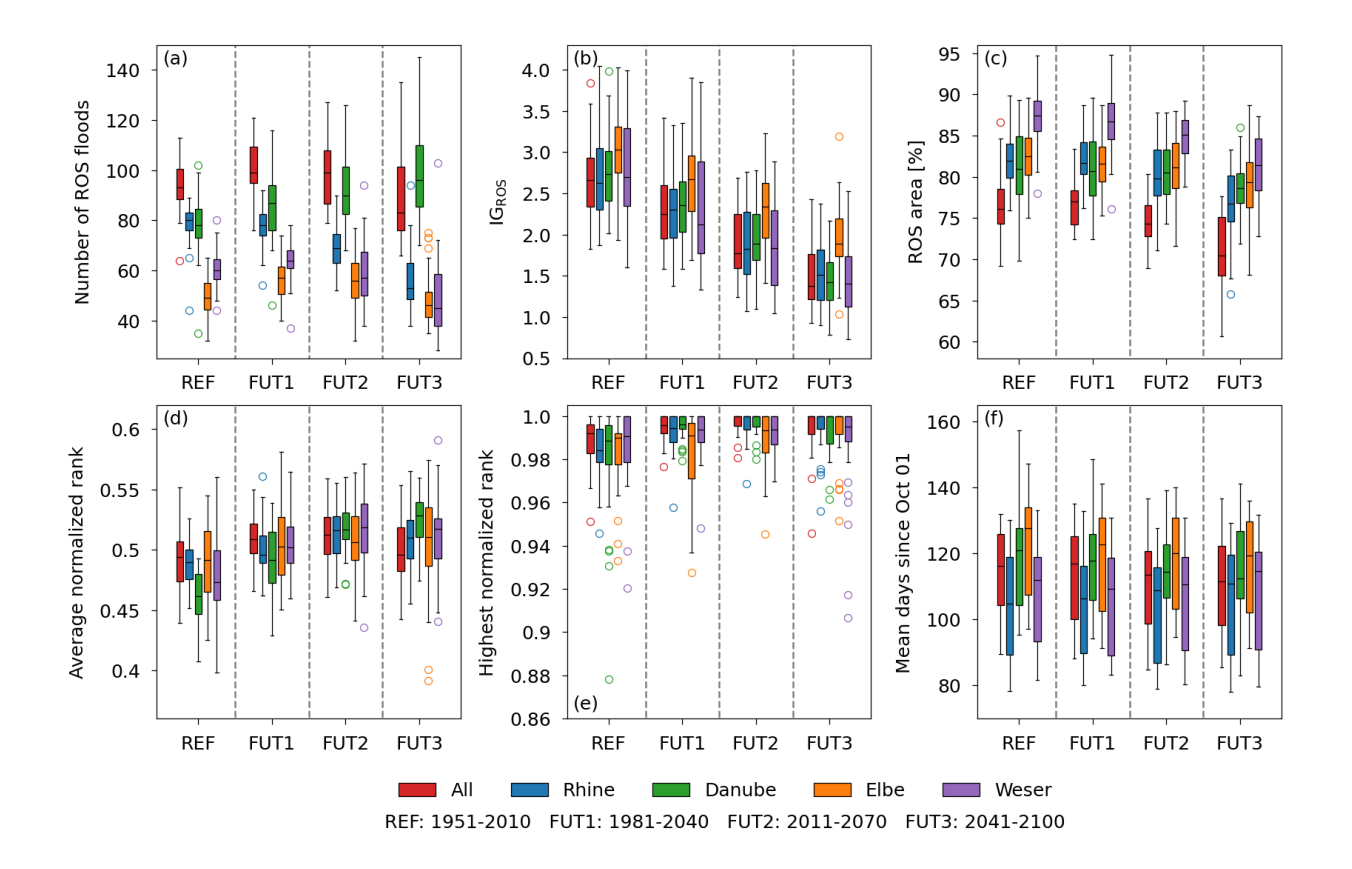


Figure 11. ROS flood properties for the RCM ensemble for the 4 time periods REF, FUT1 (1981-2040), FUT2 (2011-2070) and FUT3 (2041-2100). The number of trans-basin ROS floods (a), the mean importance of snowmelt IG_{ROS} (b), the mean area affected by ROS floods (c), the mean normalized rank (d), the maximum normalized rank (e) and the mean ROS flood date (f). The boxes represent the 25th to 75th percentile with the median as line within the box. The whiskers show 1.5 times the inter quartile range. Outliers are shown by the colored circles.

In Fig. 12(b), the decreasing trend for the Rhine, Weser, and Elbe River basins begins around 2040 to 2050. Until the 1990s, the numbers are increasing and remain stable until 2040. At the same time, the number of non-ROS trans-basin floods (Fig. 12(a)) is increasing for all basins except the Danube River basin throughout the entire time series. The numbers for the Danube River basin start to increase only after the 2090s. In total, the number of all trans-basin floods is increasing throughout the time period, but the fraction of ROS floods decreases from 60% (Elbe) and 80% (all other basins) for the ensemble mean to 40% (all basins except Danube). The ROS fraction for the Danube River basin remains high at 80%.

The IG_{ROS} value (Fig. 11 (b)) is significantly decreasing for all basins, dropping from a median between 2.75 and 3 in the REF period to a median between 1.5 and 2 in the 2041-2100 period, indicating a clear trend towards a more rain-driven ROS floods. In all periods, ROS floods in the Elbe River basin are more snowmelt-driven compared to those in the other basins. Alongside the decreasing trend in the importance of snowmelt, the proportion of the flood area affected by ROS is also declining (Fig.



385

390

395

400



11 (c)). Most basins experience a reduction of 5 to 10 percentage points in the median until the 2041-2100 period. During the 1981-2040 and 2011-2070 periods, the ROS-affected area remains relatively stable for the Rhine, Danube, and Elbe River, only starting to decline in the 2041-2100 period. The ROS-affected area for the Weser River basin is already decreasing during the 2011-2070 period. For the Danube River basin, this trend is not significant (p = 0.052).

For the mean and maximum normalized rank (Fig. 11 (d) and (e)), an increase is projected at least until the 2011-2070 period. The mean rank for the 2041-2100 period shows a further increase for the Danube River basin and a slight decrease for the Rhine River basin as well as for all basins combined. The maximum rank displays higher values for all future periods compared to the REF period. However, they are very similar to one another, except for the Elbe River basin, which exhibits a wide model spread, particularly for the 1981-2040 period. In terms of model spread, for the 2041-2100 period, the maximum rank appears to be lower for some models than for the 2011-2070 period. The changes in mean rank are significant until the 2011-2070 period for all major basins. For the 2041-2100 period, the changes are not significant for the Elbe River basin due to the larger model spread and for all basins combined due to the decrease in rank. Except for the Weser River basin, the changes in maximum rank are significant for the 2041-2100 period. While the exact amount of the increase in magnitude cannot be determined solely by considering rank as a measure, the trend towards stronger ROS floods is clear.

The trend for the average timing of ROS floods (Fig. 11 (f)) is not as clear as for the other characteristics. For the Danube and Elbe River basins, the ensemble median projects a shift of 10 days to earlier dates. In contrast, the Weser River basin shows almost no change, while the Rhine River basin is projected to experience a shift to later dates. However, the model spread for the 25th to 75th percentiles remains similar, and there is no significant difference between the ensemble across all periods.

This is also reflected in the change in seasonality of trans-basin ROS floods. Figure 13 illustrates the fraction of trans-basin ROS floods for each month for the REF and 2041-2100 periods. The distribution of ROS floods for the REF period is similar to that of the ERA5-driven simulation, but with a maximum in January instead of February. All basins exhibit strong seasonality with almost no ROS floods from May to September in the median, except for the Danube River basin, where ROS floods occur frequently during May and September. For the Elbe River basin, the seasonality is weaker, with many ROS floods occurring in February and March. In some models within the 10th and 90th percentiles, ROS floods can be found in summer, especially for the Danube River basin. For the 2041-2100 period, the seasonality tends to become slightly stronger for all basins, with the largest change occurring in the median for the Elbe River basin and for the Danube River basin when considering individual models from the 10th to 90th percentiles.

Diverging trends and discrepancies among some of the individual models are also apparent on the trans-basin scale. This is most evident in the frequency and in the maximum rank of trans-basin ROS floods. As with the individual gauges, the reasons for the diverging trends will be discussed at the end of the section.

In Fig. 12, the time series for the number of ROS floods shows distinct periods with a high number of floods and periods with fewer floods. This behavior was previously noted by Tarasova et al. (2023), who investigated the change in flood-generating processes using observations between 1960 and 2010 in Europe. Figure A2 shows the time series of ROS trans-basin floods grouped by the driving GCMs of the climate simulations. While the different RCMs show some contribution to the frequency



420

430



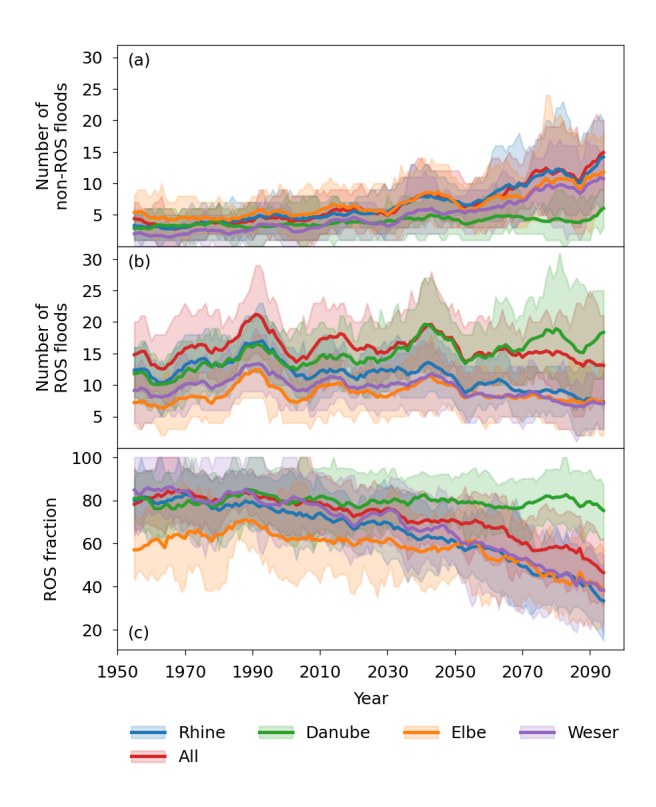


Figure 12. Rolling 10-year sum of non-ROS trans-basin floods (a), ROS trans-basin floods (b), and the fraction of ROS floods with respect to all trans-basin floods(c) for the Rhine, Danube, Elbe, and Weser River basins as well as for all basins combined during all months.

of ROS trans-basin floods, the general trend and periods of high and low amounts of ROS floods are dominated by the driving GCM. These periods of high and low numbers of ROS trans-basin floods appear in both the historical period and the future, indicating that persistent periods of many ROS floods may still be present in a future warming climate.

Previous studies identified flood-rich and flood-poor periods in observational data (e.g., Schmocker-Fackel and Naef, 2010; Villarini et al., 2013; Merz et al., 2016; Fischer et al., 2023), which appear to be primarily caused by catchment memory effects rather than decadal climate variability (Schmocker-Fackel and Naef, 2010; Merz et al., 2016). However, for the USA, Villarini et al. (2013) observe a correlation between flood-rich and flood-poor periods and large-scale climate indices such as the North Atlantic Circulation (NAO)-Index. Note that these studies mainly focus on flood events with a high magnitude. In this study, flood events with a variety of flood magnitudes are considered. However, the attribution of the flood-rich and flood-poor periods found in this study to the decadal variability of large-scale climate drivers is supported by studies that have identified a correlation between the frequency of ROS events and the NAO and the Arctic Oscillation (AO) (e.g., Cohen et al., 2015). Additionally, other studies attribute lower snow heights to a positive phase of the NAO (e.g. Hurrell, 1995) and find larger snow amounts primarily during negative phases of the NAO (e.g. Krug et al., 2020). Furthermore, Comas-Bru and McDermott (2014) point out the importance of the Eastern Atlantic pattern (EA) and the Scandinavian pattern (SCA) on the winter climate



435



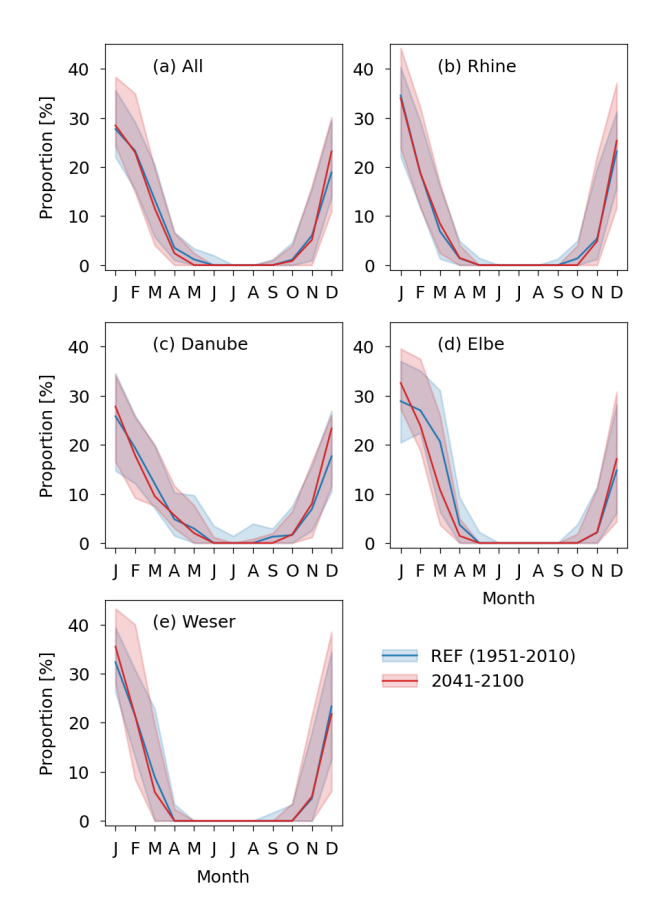


Figure 13. Seasonality of trans-basin ROS floods for all basins (a), and the Rhine (b), Danube (c), Elbe (d), and Weser (e) River basins for the REF period and 2041-2100. The lines show the fraction of total trans-basin ROS floods per month for the ensemble median. The shaded area denotes the 10th to 90th percentile.

conditions in Europe. The dominant characteristics of the GCMs further support a correlation of ROS flood frequency and NAO and AO, since the GCMs are initialized differently and are in different phases of large-scale climate patterns such as NAO and AO (note that in Fig. A2, the MPI-M-MPI-ESM-LR-GERICS-REMO2015 driven LSTM simulation was excluded, because a different GCM ensemble member (r3i1p1 instead of r1i1p1) was used and thus the phases did not match) (Taylor et al., 2012).

This motivates further investigation of a generating-process-based relationship between flood frequency and large-scale climatic drivers without dependence on flood magnitude.





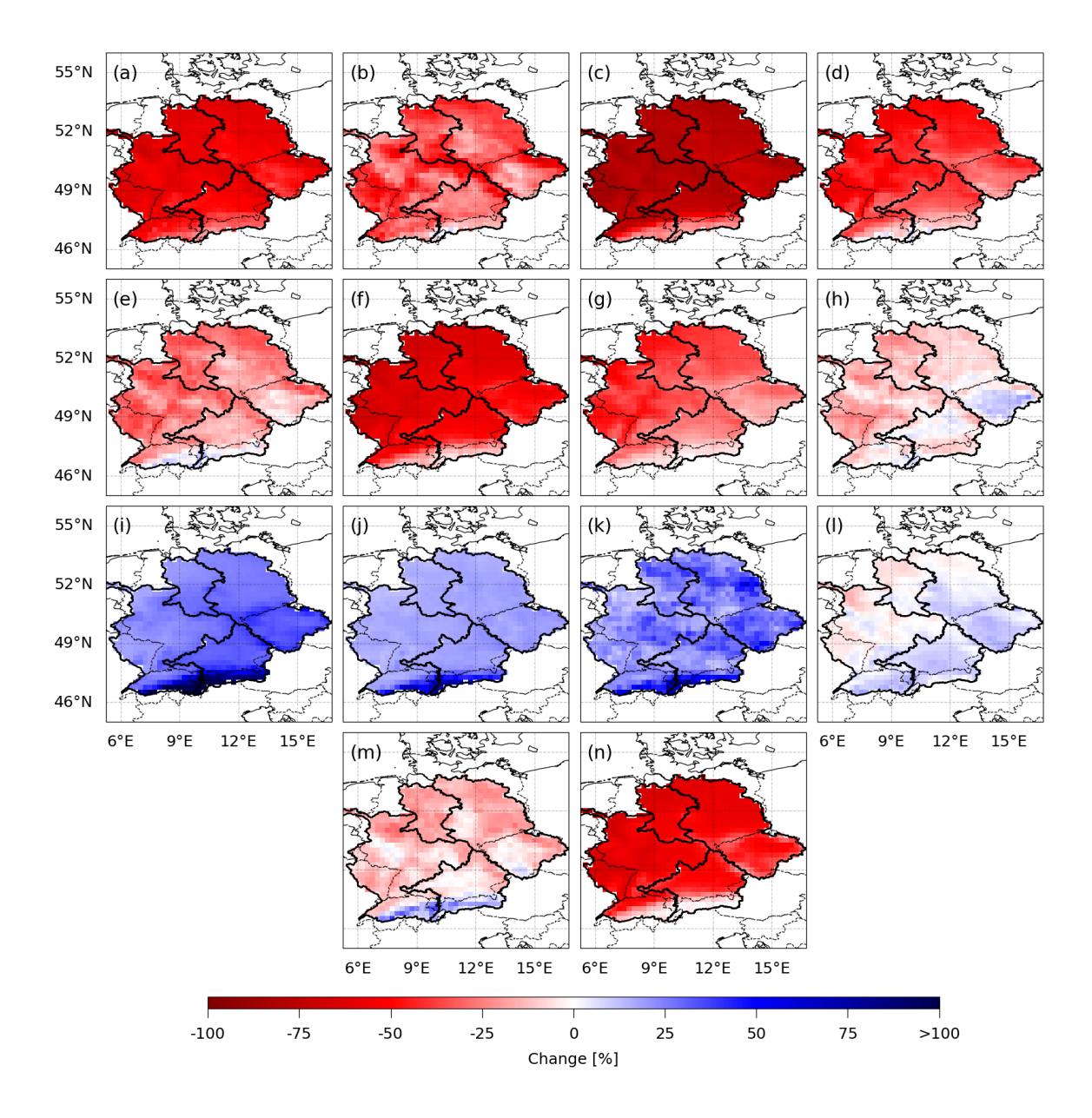


Figure 14. Ensemble mean of relative changes of selected atmospheric variables for 2041-2100 compared to the REF period. Mean annual maximum snow amount (a), maximum snow amount (b), mean annual snow days (snow amount > 15mmSWE) (c), mean October to May maximum 5-day snowmelt (d), maximum October to May 5-day snowmelt (e), mean October to May snowfall amount (f), mean October to May be liquid precipitation amount (h), mean October to May 5-day precipitation amount (j), maximum October to May 5-day precipitation amount (k), mean October to May 5-day precipitation amount (k), mean ROS water (5-day sum of liquid precipitation and snowmelt if ROS conditions are met) (l), maximum ROS water (5-day sum of liquid precipitation and snowmelt are smaller than 0.1.



450

460



440 3.3 Change of atmospheric variables

Changes in ROS events, as a flood-generating process, can be attributed to changes in rainfall and snow accumulation (Freudiger et al., 2014). Figure 14 shows the mean changes in snow amount, snowmelt, snowfall and liquid precipitation from the model ensemble as described in Table 1, for the 2041-2100 period relative to the REF period (See Figs. S8 and S9 for the periods 1981-2040 and 2011-2070). For all snow-related variables, there is a clear decrease in both the mean annual maxima and the maxima over the specified time periods. The changes in the mean annual maxima are more pronounced, as very rare extreme events are still projected to occur in the future.

The mean annual winter snowfall is projected to decrease across the entire study area, which will also impact annual maxima in snow amount and snowmelt. Notably, the annual number of snow days with a snow cover exceeding 15mmSWE is decreasing significantly. The smallest projected decrease is found in the Alps for all snow-related variables. For the period maxima, additional regions outside of the Alps show lower decreases or, in the case of 5-day snowfall, even an increase. These regions are located in the Czech and midwestern parts of the Elbe River basin, the Danube River basin, and the northern and eastern parts of the Rhine River basin. In these areas, some models project extremes that exceed a 100% increase compared to the REF period.

In contrast to the snow-related variables, liquid precipitation is projected to increase in winter, both in terms of mean values and extremes, exceeding 100% in the Alps. The mean 5-day ROS water (i.e. the 5-day sum of liquid precipitation and snowmelt) is therefore only decreasing in certain areas of the Rhine River basin and the northern parts of the Weser and Elbe River basins. While ROS water extremes are decreasing, this decline is not as pronounced as that of the snow-related variables. The increase in liquid precipitation can compensate for most of the loss in snowmelt. However, ROS events (defined here as events with ratios of 5-day liquid precipitation and 5-day snowmelt < 0.1) are significantly declining. This is also in line with the decline in ROS frequency in observations (Freudiger et al., 2014) and a projected decline in ROS frequency for a future SSP5-85 scenario (Maina and Kumar, 2025). However, in their study, the decrease in the Alps is smaller than in the lower-elevated regions.

Although the trends of the variables generally align with the trends in ROS properties, such as a decrease in the importance of snowmelt, a decline in ROS frequency at most gauges, and a slight increase in mean magnitude for the ensemble median, this alignment is not apparent for the extremes. Outside of the Alps, there are no regions showing an increase in maximum 5-day ROS water for the ensemble median. Additionally, for the individual models, the patterns of projected changes in maximum ROS flood rank do not correspond with the projected changes in maximum 5-day ROS water. Increase winter precipitation may lead to more frequent soil saturation and potentially higher mean streamflow, which could enhance extreme flood events. The diverging trends in ROS floods among the individual models may seem surprising initially, as all trends in the variables shown in Fig. 14 (except for the extreme values for each period) share the same direction and a similar magnitude (Figs. S10-S23). However, the snow dynamics vary significantly between the models. While the general patterns of snow and precipitation distributions align well, there is considerable variability in the initial conditions during the REF period and the projected future values for the 2041-2100 period. For example, the RCMs driven by CNRM-CERFACS-CNRM-CM5 and the GCMs

https://doi.org/10.5194/egusphere-2025-3532 Preprint. Discussion started: 10 November 2025





475

480

485

490

495



downscaled by KNMI-RACMO22E produce a high number of ROS events in the REF period (Figs S24) and maintain high numbers in the 2041-2100 period (Fig. S25). The relative trend is similar to that of the other models (Fig. S23). The extreme increase in ROS frequency of the CNRM-CERFACS-CNRM-CM5 GERICS-REMO2015 setup can be attributed to a very high frequency of snowmelt floods in the REF period (Fig. S26), which transform to ROS floods in a warming climate. Changes in ROS properties resulting from such extreme changes in ROS frequency are most likely due to statistical reasons.

For the other models, the explanation is not as straightforward. However, RCMs driven by the same GCM and GMCs driving the same RCM often exhibit a similar behavior.

The high variability between climate models in terms of projected flood changes has been highlighted in numerous other studies (e.g., Smith et al., 2014; Camici et al., 2014). Sezen et al. (2020) addressed this issue concerning changes in ROS frequency and magnitude. They also emphasize that in addition to changes in meteorological conditions, factors not included in the GCMs and RCMs, such as changes in land use, could further influence future ROS floods.

The results of this study are based on an RCP8.5 scenario from the CORDEX CMIP5 experiment. With possible limitations of LSTM in their ability to extrapolate and simulate unseen events, we mainly focus on the change in flood-generating processes using XAI and assess possible changes in flood magnitude by a comparison of flood ranks, and thus provide the possibility of a change rather than the actual change in peak discharge. Therefore, we believe that our results are reliable within these limitations.

For recent CMIP6 global climate projections, the less pessimistic SSP3-7.0 emission scenario is used as the high-impact scenario to drive the RCMs in the CORDEX. Under this emission scenario, the projected changes of the 2041-2100 period could potentially be lower in the CORDEX CMIP6 ensemble and may resemble the changes found for the 2011-2070 period at the end of the century. (Maina and Kumar, 2025) highlight that during a transition phase with decreasing snow cover and increasing precipitation, ROS events can potentially trigger large amounts of snowmelt. In a less pessimistic scenario, the duration of such a transition phase is potentially longer and therefore poses an increased risk of severe ROS floods.

4 Conclusions

In this study, we analyzed the changes in frequency, severity, and properties of rain-on-snow (ROS) floods in Germany. We used 31 combinations of global and regional climate models to simulate future streamflow under the RCP8.5 high-emission scenario at 96 river gauges in Germany, using a Long-Short-Term Model that was trained to reproduce past streamflow observations when driven by the ERA5 reanalysis. The model demonstrated an accurate representation of flood timing, and its ability to simulate flood events, despite generally underestimating their magnitudes, warranted the use of a novel explainable artificial intelligence technique to identify floods generated by the ROS process.

Our findings indicate a decline in the frequency of ROS floods at the majority of individual study gauges with only a few projected increases win the Danube and Elbe River basins. Notably, the Danube region is the only area showing a steady increase



510

515

520



in trans-basin ROS floods in the future.

Overall, ROS floods are becoming more rainfall-driven, with a corresponding decrease in the contribution of snowmelt for all individual gauges and for trans-basin floods in the study area. Consequently, the area of trans-basin floods affected by ROS is also declining.

The mean rank (as a representative of the mean magnitude within a time period) of trans-basin ROS floods shows an increase until the period from 2011 to 2070, while the maximum rank (as a representative of the highest magnitude within a time period) of ROS floods increased from the period from 1951 to 2010 towards the period from 1981 to 2040, subsequently remaining stable in more distant future periods. The maximum rank of ROS floods is projected to be higher for all basins in all future periods. Additionally, the mean rank of ROS floods increases for almost all individual gauges. However, the maximum rank increases only in most of the western Danube basin, the western Elbe, and the middle to northern Weser basin and decreases in most of the Rhine basin.

This decreasing importance of snowmelt, along with the declining ROS frequency and the increasing mean flood rank, is reflected in changes in the mean values of the corresponding atmospheric variables. While snow amount and snowmelt decrease, liquid precipitation generally increases from October to May, compensating for the loss of snowmelt. Additional factors such as increased soil moisture and higher mean winter streamflow are likely contributing to the increase of the maximum rank of ROS events.

There is a considerable variability between the models regarding the trends of ROS floods, which is related to the different dynamics of snow and precipitation in the individual climate models. This highlights the necessity for ensemble-based assessments for understanding and projecting local changes in future flood-generating processes.

Code and data availability. The ERA5 hourly data can be downloaded at the Copernicus Climate Data Store (https://cds.climate.copernicus.eu/). The downscaled CORDEX CMIP5 data are available in the ESGF data base (https://esgf-metagrid.cloud.dkrz.de/). GRDC daily river discharge data are available at https://portal.grdc.bafg.de/. The simulated streamflow, the flood-generating processes, the trained LSTMS, and the code used for the analysis and for the production of the figures are available on 10.5281/zenodo.16368450.





530 Appendix A: Appendix

Table A1. Climate simulations from the CORDEX CMIP5 ensemble.

| RCM | Version | GCM | Ensemble member | Scenario |
|------------------------------|---------|-----------------------|-----------------|--------------------|
| CLMcom-ETH-COSMO-crCLIM-v1-1 | v1 | CNRM-CERFACS-CNRM-CM5 | rlilpl | historical, RCP8.5 |
| CLMcom-ETH-COSMO-crCLIM-v1-1 | v1 | ICHEC-EC-EARTH | r12i1p1 | historical, RCP8.5 |
| CLMcom-ETH-COSMO-crCLIM-v1-1 | v1 | MOHC-HadGEM2-ES | r1i1p1 | historical, RCP8.5 |
| CLMcom-ETH-COSMO-crCLIM-v1-1 | v1 | MPI-M-MPI-ESM-LR | r1i1p1 | historical, RCP8.5 |
| CLMcom-ETH-COSMO-crCLIM-v1-1 | v1 | NCC-NorESM1-M | r1i1p1 | historical, RCP8.5 |
| CLMcom-ETH-COSMO-crCLIM-v1-1 | v1 | ECMWF-ERAINT | rlilpl | evaluation |
| CNRM-ALADIN63 | v2 | CNRM-CERFACS-CNRM-CM5 | rlilpl | historical, RCP8.5 |
| CNRM-ALADIN63 | v1 | MOHC-HadGEM2-ES | rlilp1 | historical, RCP8.5 |
| CNRM-ALADIN63 | v1 | MPI-M-MPI-ESM-LR | rlilp1 | historical, RCP8.5 |
| CNRM-ALADIN63 | v1 | NCC-NorESM1-M | rlilp1 | historical, RCP8.5 |
| CNRM-ALADIN63 | v1 | ECMWF-ERAINT | rlilpl | evaluation |
| DMI-HIRHAM5 | v2 | CNRM-CERFACS-CNRM-CM5 | rlilpl | historical, RCP8.5 |
| DMI-HIRHAM5 | v1 | ICHEC-EC-EARTH | r12i1p1 | historical, RCP8.5 |
| DMI-HIRHAM5 | v2 | MOHC-HadGEM2-ES | rlilp1 | historical, RCP8.5 |
| DMI-HIRHAM5 | v1 | MPI-M-MPI-ESM-LR | rli1p1 | historical, RCP8.5 |
| DMI-HIRHAM5 | v3 | NCC-NorESM1-M | r1i1p1 | historical, RCP8.5 |
| DMI-HIRHAM5 | v1 | ECMWF-ERAINT | rlilpl | evaluation |
| GERICS-REMO2015 | v1 | CCCma-CanESM2 | rlilpl | historical, RCP8.5 |
| GERICS-REMO2015 | v1 | CNRM-CERFACS-CNRM-CM5 | rlilp1 | historical, RCP8.5 |
| GERICS-REMO2015 | v1 | ICHEC-EC-EARTH | r12i1p1 | historical, RCP8.5 |
| GERICS-REMO2015 | v1 | MIROC-MIROC5 | rlilp1 | historical, RCP8.5 |
| GERICS-REMO2015 | v1 | MOHC-HadGEM2-ES | r1i1p1 | historical, RCP8.5 |
| GERICS-REMO2015 | v1 | MPI-M-MPI-ESM-LR | rlilp1 | historical, RCP8.5 |
| GERICS-REMO2015 | v1 | NCC-NorESM1-M | r1i1p1 | historical, RCP8.5 |
| GERICS-REMO2015 | v1 | ECMWF-ERAINT | rlilpl | evaluation |
| KNMI-RACMO22E | v2 | CNRM-CERFACS-CNRM-CM5 | rlilpl | historical, RCP8.5 |
| KNMI-RACMO22E | v1 | ICHEC-EC-EARTH | r12i1p1 | historical, RCP8.5 |
| KNMI-RACMO22E | v2 | MOHC-HadGEM2-ES | rli1p1 | historical, RCP8.5 |
| KNMI-RACMO22E | v1 | MPI-M-MPI-ESM-LR | r1i1p1 | historical, RCP8.5 |
| KNMI-RACMO22E | v1 | NCC-NorESM1-M | r1i1p1 | historical, RCP8.5 |
| KNMI-RACMO22E | v1 | ECMWF-ERAINT | rlilpl | evaluation |
| MOHC-HadREM3-GA7-05 | v2 | CNRM-CERFACS-CNRM-CM5 | rlilpl | historical, RCP8.5 |
| MOHC-HadREM3-GA7-05 | v1 | ICHEC-EC-EARTH | r12i1p1 | historical, RCP8.5 |
| MOHC-HadREM3-GA7-05 | v1 | MOHC-HadGEM2-ES | rlilpl | historical, RCP8.5 |
| MOHC-HadREM3-GA7-05 | v1 | MPI-M-MPI-ESM-LR | rlilpl | historical, RCP8.5 |
| MOHC-HadREM3-GA7-05 | v1 | NCC-NorESM1-M | rlilpl | historical, RCP8.5 |
| MOHC-HadREM3-GA7-05 | v1 | ECMWF-ERAINT | rlilp1 | evaluation |

All simulation data can be downloaded at https://esgf-metagrid.cloud.dkrz.de/.





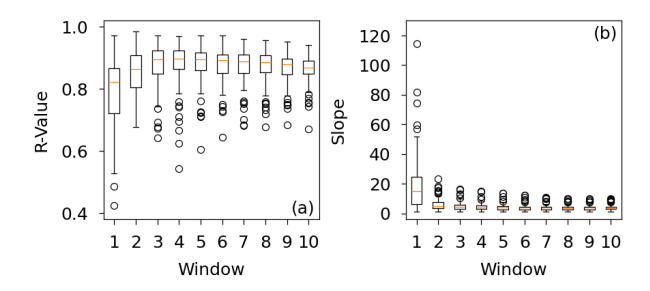


Figure A1. Correlation (a), and slope of the regression line (b) for the XAI-based IG_{ROS} value and the ratio of snowmelt and liquid precipitation of ERA5 for ROS POT5 peaks using different time windows for the XAI-based classification.

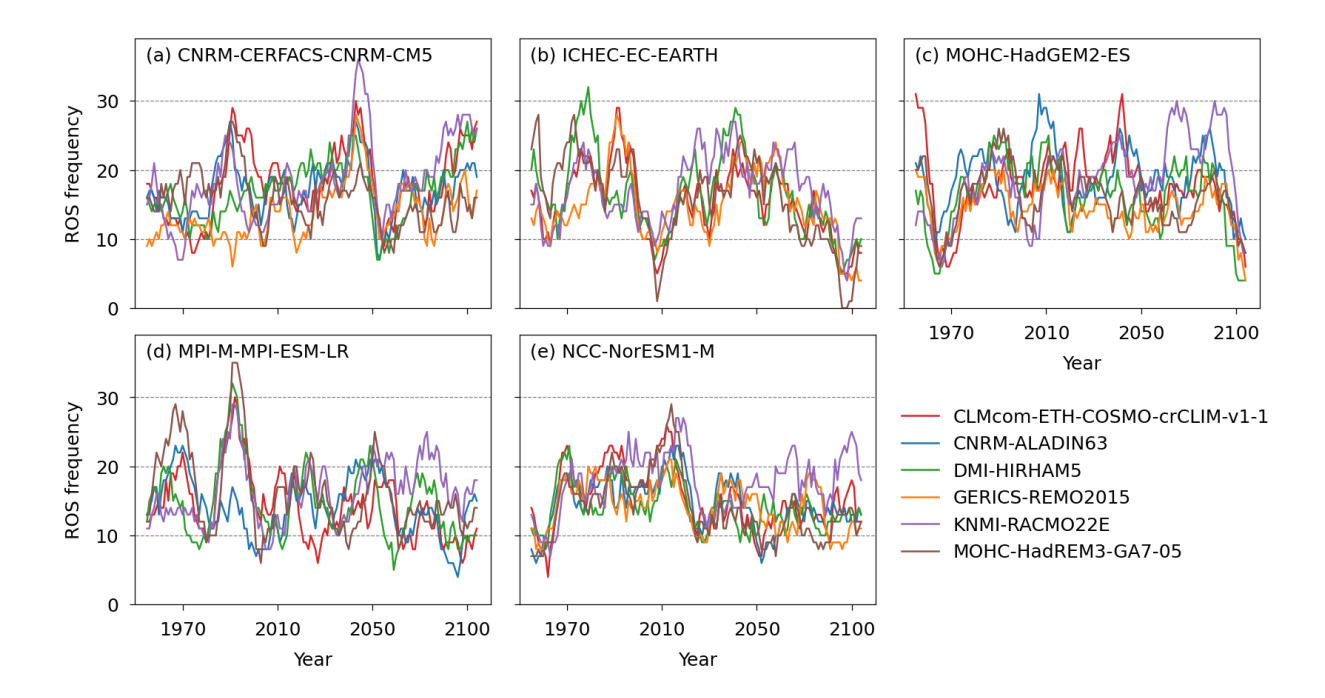


Figure A2. Rolling 10-year sum of ROS trans-basin floods detected in the streamflow simulations of the individual climate models for all basins combined during all months. The different panels show the number of ROS trans-basin floods for different driving GCMs. (a) CNRM-CERFACS-CNRM-CM5, (b) ICHEC-EC-EARTH, (c) MOHC-HadGEM2-ES, (d) MPI-M-MPI-ESM-LR, and (e) NCC-NorESM1-M. The CCma-CanESM2 MIROC-MIROC5 GCMs and the MPI-M-MPI-ESM-LR-GERICS-REMO2015 simulation were excluded.

Author contributions. CC and BA determined the research outline. BA acquired funding. CC and LT acquired the data. CC wrote the code and performed the calculations and analysis of the results, BA and LT provided guidance on the analysis. CC wrote the initial draft, BA and LT reviewed and edited the manuscript.





Competing interests. The authors declare that they have no conflict of interest.

535 Acknowledgements. The financial support of the German Research Foundation (Deutsche Forschungsgemeinschaft, DFG) in terms of the research group FOR 2416 Space-Time Dynamics of Extreme Floods (SPATE) is gratefully acknowledged. Computational resources were provided by the Center for Scientific Computing (CSC) Frankfurt. The authors thank the European Centre for Medium-Range Weather Forecasts (ECMWF) for providing the ERA5 reanalysis data, all participating institutes of the CORDEX CMIP5 ensemble for performing the climate simulations and providing their data, and the Earth System Grid Federation for access to the data through their infrastructure. 540

Furthermore, the authors thank the Global Runoff Data Centre (56068 Koblenz, Germany) for providing the river discharge data.





References

545

550

560

575

- Beniston, M. and Stoffel, M.: Rain-on-snow events, floods and climate change in the Alps: Events may increase with warming up to 4°C and decrease thereafter, Science of The Total Environment, 571, 228–236, https://doi.org/10.1016/j.scitotenv.2016.07.146, 2016.
- Bertola, M., Viglione, A., Lun, D., Hall, J., and Blöschl, G.: Flood trends in Europe: are changes in small and big floods different?, Hydrology and Earth System Sciences, 24, 1805–1822, https://doi.org/10.5194/hess-24-1805-2020, 2020.
- Blöschl, G., Hall, J., Viglione, A., Perdigão, R. A., Parajka, J., Merz, B., Lun, D., Arheimer, B., Aronica, G. T., Bilibashi, A., et al.: Changing climate both increases and decreases European river floods, Nature, 573, 108–111, https://doi.org/10.1038/s41586-019-1495-6, 2019.
- Blöschl, G., Hall, J., Parajka, J., Perdigão, R. A. P., Merz, B., Arheimer, B., Aronica, G. T., Bilibashi, A., Bonacci, O., Borga, M., Čanjevac, I., Castellarin, A., Chirico, G. B., Claps, P., Fiala, K., Frolova, N., Gorbachova, L., Gül, A., Hannaford, J., Harrigan, S., Kireeva, M., Kiss, A., Kjeldsen, T. R., Kohnová, S., Koskela, J. J., Ledvinka, O., Macdonald, N., Mavrova-Guirguinova, M., Mediero, L., Merz, R., Molnar, P., Montanari, A., Murphy, C., Osuch, M., Ovcharuk, V., Radevski, I., Rogger, M., Salinas, J. L., Sauquet, E., Šraj, M., Szolgay, J., Viglione, A., Volpi, E., Wilson, D., Zaimi, K., and Živković, N.: Changing climate shifts timing of European floods, Science, 357, 588–590, https://doi.org/10.1126/science.aan2506, 2017.
- Camici, S., Brocca, L., Melone, F., and Moramarco, T.: Impact of Climate Change on Flood Frequency Using Different Climate Models and
 Downscaling Approaches, Journal of Hydrologic Engineering, 19, 04014 002, https://doi.org/10.1061/(ASCE)HE.1943-5584.0000959,
 2014.
 - Cannon, A. J., Sobie, S. R., and Murdock, T. Q.: Bias Correction of GCM Precipitation by Quantile Mapping: How Well Do Methods Preserve Changes in Quantiles and Extremes?, Journal of Climate, 28, 6938 6959, https://doi.org/10.1175/JCLI-D-14-00754.1, 2015.
 - Chegwidden S, O., Rupp, D. E., and Nijssen, B.: Climate change alters flood magnitudes and mechanisms in climatically-diverse headwaters across the northwestern United States, Environmental Research Letters, 15, 094 048, https://doi.org/10.1088/1748-9326/ab986f, 2020.
 - Cohen, J., Ye, H., and Jones, J.: Trends and variability in rain-on-snow events, Geophysical Research Letters, 42, 7115–7122, https://doi.org/10.1002/2015GL065320, 2015.
 - Comas-Bru, L. and McDermott, F.: Impacts of the EA and SCA patterns on the European twentieth century NAO–winter climate relationship, Quarterly Journal of the Royal Meteorological Society, 140, 354–363, https://doi.org/10.1002/qj.2158, 2014.
- Dee, D. P., Uppala, S. M., Simmons, A. J., Berrisford, P., Poli, P., Kobayashi, S., Andrae, U., Balmaseda, M. A., Balsamo, G., Bauer, P., Bechtold, P., Beljaars, A. C. M., van de Berg, L., Bidlot, J., Bormann, N., Delsol, C., Dragani, R., Fuentes, M., Geer, A. J., Haimberger, L., Healy, S. B., Hersbach, H., Hólm, E. V., Isaksen, L., Kållberg, P., Köhler, M., Matricardi, M., McNally, A. P., Monge-Sanz, B. M., Morcrette, J.-J., Park, B.-K., Peubey, C., de Rosnay, P., Tavolato, C., Thépaut, J.-N., and Vitart, F.: The ERA-Interim reanalysis: configuration and performance of the data assimilation system, Quarterly Journal of the Royal Meteorological Society, 137, 553–597, https://doi.org/10.1002/qj.828, 2011.
 - Dong, C. and Menzel, L.: Recent snow cover changes over central European low mountain ranges, Hydrological Processes, 34, 321–338, https://doi.org/10.1002/hyp.13586, 2020.
 - Fischer, S., Lun, D., Schumann, A. H., and Blöschl, G.: Detecting flood-type-specific flood-rich and flood-poor periods in peaks-over-threshold series with application to Bavaria (Germany), Stochastic Environmental Research and Risk Assessment, 37, 1395–1413, https://doi.org/10.1007/s00477-022-02350-8, 2023.
 - Freudiger, D., Kohn, I., Stahl, K., and Weiler, M.: Large-scale analysis of changing frequencies of rain-on-snow events with flood-generation potential, Hydrology and Earth System Sciences, 18, 2695–2709, https://doi.org/10.5194/hess-18-2695-2014, 2014.





- Hersbach, H., Bell, B., Berrisford, P., Hirahara, S., Horányi, A., Muñoz-Sabater, J., Nicolas, J., Peubey, C., Radu, R., Schepers, D., Simmons, A., Soci, C., Abdalla, S., Abellan, X., Balsamo, G., Bechtold, P., Biavati, G., Bidlot, J., Bonavita, M., De Chiara, G., Dahlgren, P., Dee, D., Diamantakis, M., Dragani, R., Flemming, J., Forbes, R., Fuentes, M., Geer, A., Haimberger, L., Healy, S., Hogan, R. J.,
- P., Dee, D., Diamantakis, M., Dragani, R., Flemming, J., Forbes, R., Fuentes, M., Geer, A., Haimberger, L., Healy, S., Hogan, R. J., Hólm, E., Janisková, M., Keeley, S., Laloyaux, P., Lopez, P., Lupu, C., Radnoti, G., de Rosnay, P., Rozum, I., Vamborg, F., Villaume, S., and Thépaut, J.-N.: The ERA5 global reanalysis, Quarterly Journal of the Royal Meteorological Society, 146, 1999–2049, https://doi.org/10.1002/qj.3803, 2020.
- Hochreiter, S. and Schmidhuber, J.: Long Short-Term Memory, Neural Comput., 9, 1735–1780, https://doi.org/10.1162/neco.1997.9.8.1735, 1997.
 - Huang, H., Fischella, M. R., Liu, Y., Ban, Z., Fayne, J. V., Li, D., Cavanaugh, K. C., and Lettenmaier, D. P.: Changes in Mechanisms and Characteristics of Western U.S. Floods Over the Last Sixty Years, Geophysical Research Letters, 49, e2021GL097022, https://doi.org/10.1029/2021GL097022, 2022.
- Hurrell, J. W.: Decadal Trends in the North Atlantic Oscillation: Regional Temperatures and Precipitation, Science, 269, 676–679, https://doi.org/10.1126/science.269.5224.676, 1995.
 - Jiang, S., Bevacqua, E., and Zscheischler, J.: River flooding mechanisms and their changes in Europe revealed by explainable machine learning, Hydrology and Earth System Sciences, 26, 6339–6359, https://doi.org/10.5194/hess-26-6339-2022, 2022a.
 - Jiang, S., Zheng, Y., Wang, C., and Babovic, V.: Uncovering Flooding Mechanisms Across the Contiguous United States Through Interpretive Deep Learning on Representative Catchments, Water Resources Research, 58, https://doi.org/10.1029/2021WR030185, 2022b.
- Kemter, M., Merz, B., Marwan, N., Vorogushyn, S., and Blöschl, G.: Joint Trends in Flood Magnitudes and Spatial Extents Across Europe, Geophysical Research Letters, 47, e2020GL087 464, https://doi.org/https://doi.org/10.1029/2020GL087464, 2020.
 - Kingma, D. P. and Ba, J.: Adam: A Method for Stochastic Optimization, https://doi.org/10.48550/arXiv.1412.6980, 2017.
 - Kratzert, F., Klotz, D., Brenner, C., Schulz, K., and Herrnegger, M.: Rainfall-runoff modelling using Long Short-Term Memory (LSTM) networks, Hydrology and Earth System Sciences, 22, 6005–6022, https://doi.org/10.5194/hess-22-6005-2018, 2018.
- Krug, A., Primo, C., Fischer, S., Schumann, A., and Ahrens, B.: On the temporal variability of widespread rain-on-snow floods, Meteorologische Zeitschrift, 29, 147–163, https://doi.org/10.1127/metz/2020/0989, 2020.
 - Li, D., Lettenmaier, D. P., Margulis, S. A., and Andreadis, K.: The Role of Rain-on-Snow in Flooding Over the Conterminous United States, Water Resources Research, 55, 8492–8513, https://doi.org/10.1029/2019WR024950, 2019.
- Maina, F. Z. and Kumar, S. V.: Diverging Trends in Rain-On-Snow Over High Mountain Asia, Earth's Future, 11, e2022EF003 009, https://doi.org/10.1029/2022EF003009, 2023.
 - Maina, F. Z. and Kumar, S. V.: Global patterns of rain-on-snow and its impacts on runoff from past to future projections, Nature Communications, 16, 1–10, https://doi.org/https://doi.org/10.1038/s41467-025-59855-3, 2025.
 - Mann, H. B. and Whitney, D. R.: On a test of whether one of two random variables is stochastically larger than theother, The annals of mathematical statistics, pp. 50–60, 1947.
- 610 Mazurkiewicz, A. B., Callery, D. G., and McDonnell, J. J.: Assessing the controls of the snow energy balance and water available for runoff in a rain-on-snow environment, Journal of Hydrology, 354, 1–14, https://doi.org/10.1016/j.jhydrol.2007.12.027, 2008.
 - McCabe, G. J., Clark, M. P., and Hay, L. E.: Rain-on-Snow Events in the Western United States, Bulletin of the American Meteorological Society, 88, 319 328, https://doi.org/10.1175/BAMS-88-3-319, 2007.
- Merz, B., Nguyen, V. D., and Vorogushyn, S.: Temporal clustering of floods in Germany: Do flood-rich and flood-poor periods exist?, Journal of Hydrology, 541, 824–838, https://doi.org/10.1016/j.jhydrol.2016.07.041, 2016.





- Merz, R. and Blöschl, G.: A process typology of regional floods, Water Resources Research, 39, https://doi.org/10.1029/2002WR001952, 2003.
- Merz, Bruno, Elmer, Florian, Kunz, Michael, Mühr, Bernhard, Schröter, Kai, and Uhlemann-Elmer, Steffi: The extreme flood in June 2013 in Germany, La Houille Blanche, pp. 5–10, https://doi.org/10.1051/lhb/2014001, 2014.
- Morán-Tejeda, E., López-Moreno, J. I., Stoffel, M., and Beniston, M.: Rain-on-snow events in Switzerland: recent observations and projections for the 21st century, Climate Research, 71, 111–125, https://doi.org/10.3354/cr01435, 2016.
 - Musselman, K. N., Lehner, F., Ikeda, K., Clark, M. P., Prein, A. F., Liu, C., Barlage, M., and Rasmussen, R.: Projected increases and shifts in rain-on-snow flood risk over western North America, Nature Climate Change, 8, 808–812, https://doi.org/10.1038/s41558-018-0236-4, 2018.
- Nash, J. and Sutcliffe, J.: River flow forecasting through conceptual models part I A discussion of principles, Journal of Hydrology, 10, 282–290, https://doi.org/10.1016/0022-1694(70)90255-6, 1970.
 - NOAA National Centers for Environmental Information: 2022: ETOPO 2022 15 Arc-Second Global Relief Model. NOAA National Centers for Environmental Information., https://doi.org/10.25921/fd45-gt74, 2022.
- Ohba, M. and Kawase, H.: Rain-on-Snow events in Japan as projected by a large ensemble of regional climate simulations, Climate Dynamics, 55, 2785–2800, https://doi.org/10.1007/s00382-020-05419-8, 2020.
 - Ondrej Hotovy, O. N. and Jenicek, M.: Changes in rain-on-snow events in mountain catchments in the rain–snow transition zone, Hydrological Sciences Journal, 68, 572–584, https://doi.org/10.1080/02626667.2023.2177544, 2023.
 - Pall, P., Tallaksen, L. M., and Stordal, F.: A Climatology of Rain-on-Snow Events for Norway, Journal of Climate, 32, 6995 7016, https://doi.org/10.1175/JCLI-D-18-0529.1, 2019.
- Petrow, T., Thieken, A. H., Kreibich, H., Merz, B., and Bahlburg, C. H.: Improvements on flood alleviation in Germany: Lessons learned from the Elbe flood in August 2002, Environmental management, 38, 717–732, https://doi.org/10.1007/s00267-005-6291-4, 2006.
 - Petrow, T., Zimmer, J., and Merz, B.: Changes in the flood hazard in Germany through changing frequency and persistence of circulation patterns, Natural Hazards and Earth System Sciences, 9, 1409–1423, https://doi.org/10.5194/nhess-9-1409-2009, 2009.
- Rojas, R., Feyen, L., Bianchi, A., and Dosio, A.: Assessment of future flood hazard in Europe using a large ensemble of bias-corrected regional climate simulations, Journal of Geophysical Research: Atmospheres, 117, https://doi.org/10.1029/2012JD017461, 2012.
 - Rössler, O., Froidevaux, P., Börst, U., Rickli, R., Martius, O., and Weingartner, R.: Retrospective analysis of a nonforecasted rain-on-snow flood in the Alps a matter of model limitations or unpredictable nature?, Hydrology and Earth System Sciences, 18, 2265–2285, https://doi.org/10.5194/hess-18-2265-2014, 2014.
- Schmocker-Fackel, P. and Naef, F.: Changes in flood frequencies in Switzerland since 1500, Hydrology and Earth System Sciences, 14, 1581–1594, https://doi.org/10.5194/hess-14-1581-2010, 2010.
 - Sezen, C., Šraj, M., Medved, A., and Bezak, N.: Investigation of Rain-On-Snow Floods under Climate Change, Applied Sciences, 10, https://doi.org/10.3390/app10041242, 2020.
 - Smith, A., Bates, P., Freer, J., and Wetterhall, F.: Investigating the application of climate models in flood projection across the UK, Hydrological Processes, 28, 2810–2823, https://doi.org/10.1002/hyp.9815, 2014.
- 650 Song, Y., Sawadekar, K., Frame, J. M., Pan, M., Clark, M., Knoben, W. J. M., Wood, A. W., Lawson, K. E., Patel, T., and Shen, C.: Physics-informed, Differentiable Hydrologic Models for Capturing Unseen Extreme Events, ESS Open Archive, https://doi.org/10.22541/essoar.172304428.82707157/v2, 2025.



655

670

680



- Stein, L., Clark, M. P., Knoben, W. J. M., Pianosi, F., and Woods, R. A.: How Do Climate and Catchment Attributes Influence Flood Generating Processes? A Large-Sample Study for 671 Catchments Across the Contiguous USA, Water Resources Research, 57, e2020WR028300, https://doi.org/https://doi.org/10.1029/2020WR028300, 2021.
- Sui, J. and Koehler, G.: Rain-on-snow induced flood events in Southern Germany, Journal of Hydrology, 252, 205–220, https://doi.org/10.1016/S0022-1694(01)00460-7, 2001.
- Sundararajan, M., Taly, A., and Yan, Q.: Axiomatic Attribution for Deep Networks, https://doi.org/10.48550/arXiv.1703.01365, 2017.
- Tarasova, L., Merz, R., Kiss, A., Basso, S., Blöschl, G., Merz, B., Viglione, A., Plötner, S., Guse, B., Schumann, A., Fischer, S.,
 Ahrens, B., Anwar, F., Bárdossy, A., Bühler, P., Haberlandt, U., Kreibich, H., Krug, A., Lun, D., Müller-Thomy, H., Pidoto, R.,
 Primo, C., Seidel, J., Vorogushyn, S., and Wietzke, L.: Causative classification of river flood events, WIREs Water, 6, e1353, https://doi.org/https://doi.org/10.1002/wat2.1353, 2019.
 - Tarasova, L., Basso, S., and Merz, R.: Transformation of Generation Processes From Small Runoff Events to Large Floods, Geophysical Research Letters, 47, e2020GL090 547, https://doi.org/10.1029/2020GL090547, 2020a.
- Tarasova, L., Basso, S., Wendi, D., Viglione, A., Kumar, R., and Merz, R.: A Process-Based Framework to Characterize and Classify Runoff Events: The Event Typology of Germany, Water Resources Research, 56, e2019WR026951, https://doi.org/10.1029/2019WR026951, 2020b.
 - Tarasova, L., Lun, D., Merz, R., Blöschl, G., Basso, S., Bertola, M., Miniussi, A., Rakovec, O., Samaniego, L., Thober, S., and Kumar, R.: Shifts in flood generation processes exacerbate regional flood anomalies in Europe, Communications Earth and Environment, 4, https://doi.org/10.1038/s43247-023-00714-8, 2023.
 - Taylor, K. E., Stouffer, R. J., and Meehl, G. A.: An Overview of CMIP5 and the Experiment Design, Bulletin of the American Meteorological Society, 93, 485 498, https://doi.org/10.1175/BAMS-D-11-00094.1, 2012.
 - Trubilowicz, J. W. and Moore, R. D.: Quantifying the role of the snowpack in generating water available for run-off during rain-on-snow events from snow pillow records, Hydrological Processes, 31, 4136–4150, https://doi.org/10.1002/hyp.11310, 2017.
- Uhlemann, S., Thieken, A. H., and Merz, B.: A consistent set of trans-basin floods in Germany between 1952–2002, Hydrology and Earth System Sciences, 14, 1277–1295, https://doi.org/10.5194/hess-14-1277-2010, 2010.
 - Ulbrich, U. and Fink, A.: The January 1995 flood in Germany: Meteorological versus hydrological causes, Physics and Chemistry of the Earth, 20, 439–444, https://doi.org/10.1016/S0079-1946(96)00002-X, 1995.
 - Ulbrich, U., Brücher, T., Fink, A. H., Leckebusch, G. C., Krüger, A., and Pinto, J. G.: The central European floods of August 2002: Part 1 Rainfall periods and flood development, Weather, 58, 371–377, https://doi.org/10.1256/wea.61.03A, 2003.
 - Villarini, G., Smith, J. A., Vitolo, R., and Stephenson, D. B.: On the temporal clustering of US floods and its relationship to climate teleconnection patterns, International Journal of Climatology, 33, 629–640, https://doi.org/10.1002/joc.3458, 2013.
 - Ye, H., Yang, D., and Robinson, D.: Winter rain on snow and its association with air temperature in northern Eurasia, Hydrological Processes, 22, 2728–2736, https://doi.org/10.1002/hyp.7094, 2008.